NASA Technical Paper 1418

A Coupled Radiative-Convective-Photochemical Model of the Stratosphere

Robert E. Boughner and John E. Nealy

APRIL 1979

NASA

NASA Technical Paper 1418

A Coupled Radiative-Convective-Photochemical Model of the Stratosphere

Robert E. Boughner and John E. Nealy
Langley Research Center
Hampton, Virginia

SUMMARY

A one-dimensional computer model of the Earth's troposphere and stratosphere is described. The model includes a photochemical reaction set of 87 kinetic processes and 28 photolytic reactions, with vertical transport being taken into account by an eddy diffusion parameter. Temperature profiles are calculated with a radiative-convective code which balances infrared atmospheric emission with solar absorption. The temperatures computed may be included in the iterative solution procedure; thus, temperature-chemistry coupling effects may be investigated. An anisotropic multiple-scattering code may also be included as a part of the coupled calculation.

The model may be used in either a direct insolation or diurnal average computation. The diurnal averaging procedures are described fully. A complete listing of the photochemical mechanism is given, along with current values for rates and cross sections. Boundary conditions for a sample calculation and the resulting vertical profiles of species concentrations and temperatures are given. It is concluded that the model gives a reasonable representation of many physical and chemical aspects of the globally averaged atmosphere.

INTRODUCTION

Study of the atmosphere is inherently complicated, involving dynamical, chemical, and radiative processes as well as their interactions. To develop a mathematical description of the atmosphere, it is necessary to understand individual processes. For this reason, atmospheric scientists have developed a hierarchy of models, each serving a specific purpose and typically concentrating on one aspect of the overall problem while treating other aspects in a simplified manner. One-dimensional models, which represent globally averaged conditions, were designed primarily to study chemical processes. Species transport is included by using an eddy diffusion parameterization that gives the net effect of several dynamical processes (mean flow, planetary waves, etc.). Three-dimensional models, on the other hand, provide detailed treatment of dynamics, while either ignoring chemistry completely or employing very truncated chemical schemes. Despite their relatively simplistic treatment of transport, one-dimensional models have performed remarkably well in predicting the mean vertical distributions of stratospheric trace species when compared with observed profiles. Because of this fact, one-dimensional models have been used extensively in the past (see, for example, refs. 1 through 7) and, because of their computational efficiency, they will continue to be used widely to examine new kinetic mechanisms before incorporating them into more complicated models and to assess the impact of man-induced perturbations on the physical state of the atmosphere.

A one-dimensional steady-state radiative-convective-photochemical model of the atmosphere has been developed recently at the Langley Research Center to study the chemical and thermal structure of the troposphere and stratosphere. The complete chemical model extends from ground level to the approximate height of the stratopause (0-55 km). Although many questions of current interest are nonsteady (for example, the release of chlorofluoromethanes), the model was not developed to predict the state of the stratosphere, but rather was developed to investigate atmospheric phenomena, specifically coupling between thermal and chemical processes. For this purpose, a steady-state model was found to be sufficient. In addition to chemical-thermal feedback, the model also incorporates molecular scattering processes and reflection of radiation from the ground and clouds. Studies may be made of the effects of injections of nitrogen oxides, water vapor, carbon dioxide, carbon monoxide, and chlorofluoromethanes, as well as investigations of the impact of changes in solar radiation on the atmospheric thermal structure. The model is fully coupled in the sense that the calculated thermal structure is consistent with the vertical profiles of the chemical species.

This paper presents the Langley model of the atmosphere. The following features of the model are relatively completely, but concisely, described:

> System of chemical and photolytic processes
> Atmospheric radiative transfer processes
> Computation and solution methods
> Current input data
> Representative examples of calculated results

SYMBOLS

A	infrared band absorptance, m^{-1}
c_p	specific heat for constant pressure, $J-kg^{-1}-K^{-1}$
e_λ	Planck blackbody function, $W-m^{-1}$
$F(\xi,\xi)$	see equation (17), $W-m^{-2}$
F_R	radiative flux, $W-m^{-2}$
f_c	fractional cloud cover
$\bar{H}$	average pressure scale height, km
$\bar{I}$	mean intensity of radiation, $W-m^{-2}$
J_ℓ	photolysis rate for ℓth photolytic process, s^{-1}
$\mathcal{J}$	Jacobian matrix (see eqs. (16)), s^{-1}
K_z	vertical eddy diffusion coefficient, m^2-s^{-1}

2

k	Boltzmann constant, $J\text{-}K^{-1}$
k_ℓ	chemical rate coefficient for ℓth kinetic process, $m^3\text{-}s^{-1}\text{-}particle^{-1}$ or $m^6\text{-}s^{-1}\text{-}particle^{-1}$
L	chemical loss rate, s^{-1}
n	number density, $particles\text{-}m^{-3}$
P	chemical production rate, $particles\text{-}m^{-3}\text{-}s^{-1}$
p	pressure, Pa
Q	heating rate, $K\text{-}s^{-1}$
q	precipitation lifetime, s
r	ratio of nighttime to daytime average concentrations of chemical species
S	net chemical production of chemical species, $particles\text{-}m^{-3}\text{-}s^{-1}$
T	temperature, K
t	time, s
t^d	length of day, s
t^n	length of night, s
t_o	length of total diurnal cycle, 24 hr
U	unit matrix
$\vec{V}$	velocity vector, $m\text{-}s^{-1}$
z	altitude, km
α	solar zenith angle, rad
$\beta_1, \beta_2, \beta_3$	diffusion-related quantities (see eq. (13)), s^{-1}
γ	see equation (11), km^{-1}
δ	defined in equation (28)
η	quantum efficiency for photolysis
λ	wavelength of radiation, m^{-1}
ξ	dimensionless optical path length

ρ gas density, $kg\text{-}m^{-3}$

σ absorption cross section, m^2

τ dimensionless optical depth

Φ particle flux, $particles\text{-}m^{-2}\text{-}s^{-1}$

χ mole fraction

Subscripts:

a   light-absorption process

c   value with inclusion of clouds

i   chemical species

j   nodal point in numerical calculation

ℓ chemical or photolytic process

nc   clear sky condition

o   surface value

s   light-scattering process

T   value at tropopause

∞ value at top of atmosphere

Superscripts:

d   daytime value

n   nighttime value

∞ total atmospheric optical depth

    An arrow over a symbol denotes a vector. Brackets around a chemical species (e.g. $[Cl]$) denote its number density.

GOVERNING EQUATIONS

    A pictorial representation of the physical and chemical processes considered is given in figure 1. The species concentrations are governed by the standard conservation equation,

$$\frac{\partial n_i}{\partial t} + \vec{\nabla} \cdot \left(n_i \vec{V} \right) = \left(\frac{dn_i}{dt} \right)_{chem} = P_i - n_i L_i \tag{1}$$

which in the one-dimensional approximation becomes

$$\frac{\partial n_i}{\partial t} + \frac{\partial \Phi_i}{\partial z} = P_i - n_i L_i \tag{2}$$

Here the chemical source term is expressed as the difference between production P_i and loss $L_i n_i$ of the ith species. The quantity Φ_i is the vertical flux which in a one-dimensional model is parameterized as being proportional to the concentration gradient

$$\Phi_i = -nK_z \frac{\partial}{\partial z} \left(\frac{n_i}{n} \right) \tag{3}$$

where n is the total number density and K_z is the vertical diffusion coefficient and represents the effect of large-scale processes on the vertical transport of species. When the equation of state ($n = p/kT$) and an average pressure scale height $\bar{\bar{H}}$ are introduced, equation (3) may be rewritten as

$$\Phi_i = -K_z \left[\frac{\partial n_i}{\partial z} + n_i \left(\frac{1}{T} \frac{dT}{dz} + \frac{1}{\bar{\bar{H}}} \right) \right] \tag{4}$$

which is one of the more common forms of the flux expression used in one-dimensional models.

In the steady-state solution of the conservation equation, the time derivative of n_i vanishes; the equations to be solved for the species concentrations are then

$$\frac{\partial}{\partial z} \left\{ -K_z \left[\frac{\partial n_i}{\partial z} + n_i \left(\frac{1}{T} \frac{dT}{dz} + \frac{1}{\bar{\bar{H}}} \right) \right] \right\} - P_i + n_i L_i = 0 \tag{5}$$

The equations are generally coupled because the chemical production and loss terms depend on other species as well as on temperature and altitude. The

explicit finite-difference equations used in solving the species conservation equations are described in detail later.

The production and loss terms in equation (5) are calculated from specified reaction rates. For photodissociation processes, such as $AB + h\nu \rightarrow A + B$, the rates J_ℓ depend on the local solar intensity in addition to the species number densities and spectral absorption coefficients $\sigma(\lambda)$:

$$J_\ell(z) = \int_\lambda d\lambda \; \sigma_\ell(\lambda) \; \eta_\ell(\lambda) \; \bar{I}_\infty(\lambda) \; \exp\left[-\int_z^\infty \sum_i \sigma_i(\lambda) \; n_i \; \sec\alpha \; dz'\right] \quad (6)$$

where η_ℓ is the quantum efficiency, $\bar{I}_\infty$ is the mean solar intensity at the top of the model atmosphere, and α is the solar zenith angle.

Equation (6) may be used to compute the photolysis rates for a fixed sun (α = Constant) or over a diurnal cycle by using the appropriate time dependence of α. The diurnal calculation incorporates several approximations for averaging of the nonlinear product terms in the species conservation equation; these approximations are described more completely in a subsequent section.

The photodissociation rates are also affected by light-scattering processes in the atmosphere. When these effects are included, scattering factors $J_{s,\ell}/J_{a,\ell}$ are calculated from the following relation:

$$\frac{J_{s,\ell}(z)}{J_{a,\ell}(z)} = \frac{1}{J_{a,\ell}(z)}\left(\int_\lambda \bar{I}_\infty(\lambda) \; \sigma_\ell\eta_\ell \; \exp\left\{\left[\tau_s^\infty(\lambda) - \tau_s(\lambda,z) + \tau_a^\infty(\lambda)\right.\right.\right.$$

$$\left.\left.\left. - \tau_a(\lambda,z)\right] \sec\alpha\right\} \; d\lambda + \int_\lambda \bar{I}(\lambda,z) \; \sigma_\ell\eta_\ell \; d\lambda\right) \quad (7)$$

where $\bar{I}$ is the diffuse intensity integrated over all solid angles, τ_s^∞ and τ_a^∞ are the total optical depths due to scattering and absorption, and τ_s and τ_a are the optical depths due to scattering and absorption at the altitude of interest. The quantity $J_{a,\ell}$, given by equation (6), is the photolysis rate in an atmosphere which only absorbs. The first term of equation (7) represents the contribution to photolysis of the direct beam attenuated by scattering and absorption, while the second term is the contribution of radiation which has been scattered one or more times.

If the vertical temperature profile is not specified, the energy conservation equation must be introduced. In the Langley model, the vertical tempera-

ture structure is calculated with a radiative-convective code wherein only radiative transfer processes are taken into account. In this situation, the energy equation reduces to

$$Q = \frac{\partial T}{\partial t} = - \frac{1}{\rho c_p} \vec{\nabla} \cdot \vec{F}_R \qquad (8)$$

where $\vec{F}_R$ is the radiative flux vector which includes the absorption of solar radiation and the absorption and emission of infrared radiation by the optically active constituents, O_3, H_2O, and CO_2. The absorption bands of these species are included by using a band absorptance and emissivity formulation, outlined in reference 8, which avoids the time-consuming and tedious integrations with respect to frequency over several thousands of spectral lines.

Because the stratosphere is nearly in a state of radiative equilibrium, temperatures in this region are calculated by setting Q equal to 0 in equation (8). The temperature-dependent terms in $\vec{\nabla} \cdot \vec{F}_R$ are used to determine the mean thermal structure. The solar heating term in the flux divergence is multiplied by 1/2 to account for the absence of heating during the night. Within the troposphere, the temperature profile is taken to decrease with height in accordance with the mean observed tropospheric lapse rate, which approximates energy transport by convective processes and latent energy release by water vapor within the troposphere. Further details concerning the temperature calculation and coupling the radiative and photochemical codes are given in the next section.

SOLUTION METHODOLOGY

In this section, the procedures used to obtain solutions to the equations given in the preceding sections are described. To facilitate the description of the various aspects of the calculation, this section is divided into the following subsections:

> Solution to the Photochemical-Transport Equations
> Temperature Calculations
> Coupled Calculations With Temperature and Scattering-
>   Albedo Effects
> Diurnal Calculations

Solution to the Photochemical-Transport Equations

As mentioned in an earlier section, the Langley model has been used to obtain steady-state solutions for the species distributions. For this case, the conservation equation for species i reduces to

$$- \frac{d\Phi_i}{dz} + S_i = 0 \tag{9}$$

where $S_i = P_i - n_i L_i$ is the net photochemical production or loss of the ith species. Equation (9) is solved between the ground and 55 km by dividing this region into N subintervals. For the present calculations, $N = 40$ has been used. Special care is taken to insure that a computational node is placed at those points where the vertical diffusion coefficient undergoes a step discontinuity.

A flux-conserving finite-difference representation of equation (9) is obtained by integrating at the jth node between $z_j - \Delta z_{j-1}/2$ and $z_j + \Delta z_j/2$ to give

$$\Phi_{i,j-1/2} - \Phi_{i,j+1/2} + \int_{z_j - \Delta z_{j-1}/2}^{z_j + \Delta z_j/2} S_i(z') \, dz' = 0 \tag{10}$$

where $\Delta z_j = z_{j+1} - z_j$ and the subscript $j + 1/2$ refers to the midpoint between the $(j + 1)$th and jth nodes. The flux (eq. (4)) is evaluated at the midpoint between two adjacent nodes with a second-order, central-difference approximation for the first derivative, which yields

$$\Phi_{i,j+1/2} = -K_{z,j+1/2} \left[\frac{n_{i,j+1} - n_{i,j}}{\Delta z_j} + \frac{1}{2} \gamma_{j+1/2} (n_{i,j+1} + n_{i,j}) \right] \tag{11}$$

where $\gamma = \frac{1}{T} \frac{dT}{dz} + \frac{1}{H}$. An expression analogous to equation (11) can also be written for $\Phi_{i,j-1/2}$. The integral term in equation (10) is approximated as

$$\int_{z_j - \Delta z_{j-1}/2}^{z_j + \Delta z_j/2} S_i(z') \, dz' \approx \frac{1}{2} (\Delta z_{j-1} + \Delta z_j) S_{i,j} \tag{12}$$

Substitution of equations (12), (11), and the corresponding expression for $\Phi_{i,j-1/2}$ into equation (10) and rearrangement of terms yield

$$-\beta_{1,j} n_{i,j-1} + \beta_{2,j} n_{i,j} - \beta_{3,j} n_{i,j+1} - S_{i,j} = 0 \tag{13}$$

where the β's are diffusion-related quantities involving the spatial step size. In the Langley model, each species distribution is determined from its

8

own conservation equation, rather than the species being grouped into families and the families tracked. One can therefore define a vector $\vec{n}_j$ whose components represent all the unknown species concentrations at the nodal point j, and then equation (13) can be rewritten in matrix form as

$$-\beta_{1,j} U \vec{n}_{j-1} + \beta_{2,j} U \vec{n}_j - \beta_{3,j} U \vec{n}_{j+1} - \vec{S}_j = 0 \tag{14}$$

where U represents the unity matrix. Equations (13) and (14) are valid only for the interior nodes, but at the upper and lower boundaries similar expressions can be developed. For example, if number density is specified at the lower boundary, then the first term on the left side of equation (13) is a known quantity which can be transposed to the right side to give

$$\beta_{2,1} n_{i,1} - \beta_{3,1} n_{i,2} - S_{i,1} = \beta_{1,1} n_{i,0} \tag{15}$$

where $j = 0$ denotes the lower boundary. When flux is given, an expression of the same form as equation (15) results except that the right side now contains the specified flux. This latter expression and equation (15) can also be put into matrix form.

Equations (14) represent a set of equations which are nonlinear and coupled because of chemical interactions among the various species. Further nonlinearities arise if interactions between the temperature field and species distributions are allowed. For a prescribed temperature profile, equations (14) are solved by a Newton-Raphson iteration. Linearization of equations (14) about an initial species distribution $\vec{n}_j^*$ yields the following for the correction terms $\delta\vec{n}_j$:

$$\beta_{1,j} U \, \delta\vec{n}_{j-1} + (\beta_{2,j} U - J) \, \delta\vec{n}_j - \beta_{3,j} U \, \delta\vec{n}_{j+1} = -\vec{R}_j\left(\vec{n}_j^*\right) \tag{16}$$

where $\vec{R}_j$ represents the residual of equations (14). The quantity J represents the Jacobian matrix of the net chemical term at node j; that is,

$$J_{i,\ell} = \frac{\partial S_i}{\partial n_\ell}$$

Equations (16), along with the corresponding equations for the lower and upper boundaries, form a tridiagonal block system which can be solved efficiently for $\delta\vec{n}_j$ (see, for example, ref. 9). The iterations are continued until the convergence criterion is satisfied. For the Langley model, the convergence

criterion is $|\epsilon| \leqq 0.001$, where ϵ is the maximum relative change in number density between two successive iterations over all computational nodes and all species to which equation (9) is applied. The number of iterations needed for a solution depends on how close the initial distribution is to the final result, but typically 15 to 25 iterations are required.

Temperature Calculations

Given distributions of the radiatively active constituents - ozone, water vapor, and carbon dioxide - and an appropriate cloud model, one can compute a globally averaged vertical temperature structure by using a radiative-convective model. Since the radiative-convective code employed in the Langley model is the one developed in reference 8 and is described fully there, only a brief description of its essential features is presented here. For further details, the reader is referred to the original paper.

Stratospheric temperatures are calculated by assuming that the stratosphere is in radiative equilibrium; that is, the net radiative heating Q is zero. The term Q includes both longwave and solar contributions due to the various absorption bands of O_3, H_2O, and CO_2. Within the troposphere, the temperature is assumed to decrease with height in accordance with the observed globally averaged lapse rate of -6.5 K/km. The temperature calculations then reduce to finding the surface temperature, the tropopause height, and the stratospheric temperature profile. Surface temperature is determined from the condition that, at the top of the atmosphere, the net outgoing longwave flux balances the net solar flux; that is, the net radiative flux $F_R = 0$.

The stratospheric temperature distribution is given by the solution to the nonlinear, integral expression for the net radiative flux divergence. With the band absorptance formulation of reference 8, the flux divergence for a particular absorber can be written generally as

$$\frac{dF_R(\xi)}{d\xi} = -e_\lambda(0)\frac{dA(\xi)}{d\xi} - \int_0^\xi F(\xi,\xi')\ d\xi'$$

$$-\int_\xi^{\xi_T} F(\xi,\xi')\ d\xi' - \int_{\xi_T}^{\xi_O} F(\xi,\xi')\ d\xi' \tag{17}$$

where

$$F(\xi,\xi') = \frac{de_\lambda(\xi')}{d\xi'}\frac{(dA)\left(|\xi - \xi'|\right)}{d\xi}$$

10

The quantity ξ is the dimensionless optical path length, which is measured from the top of the atmosphere downward, and A is the band absorptance. Particular forms for ξ and A for the various bands of O_3, H_2O, and CO_2 are given in reference 8. The quantities ξ_T and ξ_O refer to the value of ξ at the tropopause and at the surface, respectively. The parameter e_λ is the Planck function evaluated at the band center.

Since equation (17) is an integral equation, its solution is computationally time consuming and tedious. However, in reference 8, it is shown that equation (17) may be closely approximated by the following expression:

$$\frac{dF_R(\xi)}{d\xi} = -e_\lambda(\xi)\frac{dA(\xi)}{d\xi} - \int_\xi^{\xi_T} F(\xi,\xi')\ d\xi' - \int_{\xi_T}^{\xi_O} F(\xi,\xi')\ d\xi' \qquad (18)$$

The only term in equation (17) that is neglected in equation (18) is the exchange of energy between the level ξ and the region of the stratosphere lying above this level. This exchange of energy between the level ξ and the upper region makes a small contribution when compared with the terms retained, since the absorber amount and the atmospheric pressure decrease exponentially with altitude.

Within the stratosphere, the temperature distribution is obtained by letting $Q = 0$ (i.e., radiative equilibrium) where

$$Q = Q_{H_2O} + Q_{CO_2} + Q_{O_3} + Q_s \qquad (19)$$

The quantities Q_{H_2O}, Q_{CO_2}, and Q_{O_3} denote the longwave contributions to the

radiative heating by water vapor, carbon dioxide, and ozone and are given by equations analogous to equation (18); Q_s denotes the solar heating due to absorption by H_2O, CO_2, and O_3. Use of equation (18) greatly simplifies finding the temperature distribution since equation (19) can now be treated as a nonlinear, algebraic equation, provided that the temperature at the lowest level within the stratosphere is obtained first, and then the temperature at the next higher level, and so on. The integral terms in equation (18) represent contributions from the atmospheric regions below the level ξ, which are easily evaluated if the previous procedure is followed. At each computational level, the temperature is obtained from equation (19) by employing a Newton-Raphson iteration technique. The temperature is considered to have converged when the temperature change between two successive iterations is less than 0.1 K.

As mentioned earlier, the tropopause height must also be determined. This height is taken to be the highest level within the troposphere for which the lapse rate in the layer between this level and the next higher level becomes

smaller than the specified tropospheric lapse rate; that is, $\dfrac{dT}{dz} + 6.5 \approx 0$.

This level can be found by advancing upward from an initially assumed tropopause level which lies below the expected tropopause height. Temperatures are calculated by solving equation (19). As long as the lapse rate within the layer above the assumed tropopause level exceeds the specified tropospheric lapse rate, the lapse rate is set equal to the prescribed value; this procedure is repeated, advancing from level to level, until the condition $\dfrac{dT}{dz} + 6.5 \approx 0$ is satisfied.

Thus, for a specified surface temperature, the temperature distribution is calculated by first computing the tropopause height and then calculating stratospheric temperatures beginning at the level just above the computed tropopause.

Calculation of the surface temperature involves the following steps: (1) assume a surface temperature; (2) compute the tropopause height and stratospheric temperature profile by the method just explained; (3) calculate the net radiative flux at the top of the atmosphere; and (4) calculate a new surface temperature by a Newton-Raphson technique given by

$$T_O(new) = T_O(old) - \frac{F_R}{dF_R/dT_O} \tag{20}$$

Steps 2 to 4 are repeated until the condition $F_R = 0$, which represents globally averaged conditions, is satisfied. Further elaboration on the procedures used for calculation of the temperature structure is given in reference 8.

Coupled Calculations With Temperature and Scattering-Albedo Effects

Figure 2 illustrates schematically the procedure employed to include interactions between the temperature field and species concentrations. As can be seen, the photochemical and radiative codes are maintained as separate entities, with required information (namely, species profiles, primarily O_3 and H_2O, and temperature distributions) being passed between the two program units. In addition, the temperature calculations are lagged one step behind the calculations of species concentrations. To ensure that the concentrations and temperatures are consistent with one another, the cycle (fig. 2) is continued until the temperatures from two successive profiles differ by less than 0.25 K at all altitude levels. As long as temperature coupling is moderate, this procedure works satisfactorily. For stronger coupling, the number of iterations and the computation time increase. Typically, five to seven iterations on the temperature distribution are needed for a fully converged solution.

Molecular scattering from air molecules and solar reflection from the surface and clouds are included in the calculation of species profiles according to the following procedure. For each photolysis process, the altitude variation of the ratio J_s/J_a (see eq. (7)) is computed initially with a

12

multiple-scattering code described in this section, where J_s denotes the photolysis rate when molecular scattering and albedo effects are included and J_a is the photolysis rate without these effects, that is, the photodissociation rate in a purely absorbing atmosphere. To incorporate scattering and albedo effects, this array of ratios is stored and multiplied by the values of J_a which are calculated in the photochemical code. Because of the computational demands of the multiple-scattering code, the ratio J_s/J_a is held fixed and is not reevaluated, as is done with the temperatures. This procedure is based on the assumption that J_s/J_a remains invariant to changes in the species distributions, particularly those which absorb at solar wavelengths.

The value of J_s/J_a represents the weighted mean between two calculations, one for clear sky conditions and one with clouds included; that is,

$$J_s/J_a = (1 - f_c)(J_s/J_a)_{nc} + f_c(J_s/J_a)_c \qquad (21)$$

where $(J_s/J_a)_c$ denotes the ratio for full cloud cover, $(J_s/J_a)_{nc}$ is the value for clear sky conditions, and f_c represents the fractional cloud cover, which is taken as 0.5. The value of $(J_s/J_a)_c$ is computed for a single cloud layer at some effective altitude, typically taken as 5 km.

The absorption and scattering properties of the atmosphere were calculated from the following data: total number densities of O_2 and N_2 from reference 10, O_3 number density from the mid-latitude summer distribution of reference 11 (or alternatively from a photochemical calculation without scattering), spectral intervals and cross sections of O_2 and O_3 from reference 12, solar flux from references 12 and 13, and the Rayleigh scattering cross sections from reference 14.

An anisotropic multiple scattering radiation transfer code (ref. 15) has been employed to calculate the diffuse intensity field, $\overline{I}(\lambda,z)$, at 40 equally spaced intervals between 0 and 50 km and for 110 frequency intervals between 0.175 µm and 0.735 µm. This field used in conjunction with equation (7) permits the evaluation of the scattering factors for the photodissociation processes of interest.

Diurnal Calculations

Species whose chemical lifetimes are short, less than a few hours, undergo significant variations near sunrise and sunset. Even species with lifetimes of 1/2 day, such as N_2O_5, have appreciable daily variations (ref. 16). Such variations can be important in determining the impact of perturbations on the ozone concentration for two reasons. First, use of a constant, average sun can result in underestimation of the true average concentration of a species which is particularly serious if that species is a sink for more reactive species. An example of this is N_2O_5. Calculations in reference 16 indicate that use of a 24-hour average sun underpredicts the average concentration of N_2O_5 near 25 km by roughly 2 orders of magnitude compared with results which take into account its diurnal variation. For a given total odd nitrogen concentration,

13

more N_2O_5 implies smaller concentrations of NO and NO_2 to destroy ozone. A second reason to account for diurnal variations in species concentrations is accurate calculation of nonlinear terms occurring in the loss expression for odd oxygen. For example, the rate of destruction of odd oxygen by chlorine is given by

$$L_{Cl} = 2k_{45}[ClO][O] \qquad (22)$$

where k_{45} is the rate constant for the reaction

$$(45) \quad ClO + O \rightarrow Cl + O_2$$
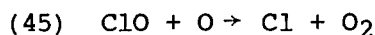
The concentration of atomic oxygen decreases rapidly at sunset by reaction with O_2 to form O_3, and when $ClONO_2$ is included in the chlorine chemical chain, the ClO concentration also decreases rapidly at sunset for altitudes below about 40 km because of reaction with NO_2 to produce $ClONO_2$ at night. Thus, the average destruction rate over 24 hours can be written as

$$L_{Cl} \approx 2k_{45} \frac{1}{2}[ClO]^d[O]^d \qquad (23)$$

where superscript d represents the daytime average. However, when a 24-hour average sun is used, the destruction rate is evaluated as

$$L_{Cl} = 2k_{45} \overline{[ClO]} \, \overline{[O]} \qquad (24)$$

with the bar denoting the 24-hour average, which, for ClO and O, is related to their daytime average value according to $\overline{n_i} = \frac{1}{2} n_i^d$. Substitution of this last result into equation (24) and comparison with equation (23) show that use of a 24-hour average sun causes the destruction rate of odd oxygen due to chlorine to be underestimated by approximately a factor of 2. This simple estimate agrees reasonably well with the more exact calculations of reference 17, indicating that the factor is 1.6 at 30 km.

To accurately account for the impact of man-induced perturbations on ozone, the diurnal effects discussed in the previous two paragraphs must be included in the calculations. However, a direct time integration of the fully time-dependent equations is impractical because of excessive demands on computer resources when model simulation times of several decades are required, as in the chlorine-ozone problem. A simpler diurnal averaging procedure is needed so that a constant sun integration reproduces the true diurnal average of the long-time integration of a fully time-dependent calculation. In this work, the averaging procedure

14

suggested in reference 18 is adopted. This method is based on the fact that species having significant diurnal variations are driven mainly by photochemistry. In addition, most of this variation occurs near sunrise and sunset, while over a major portion of the day and night the variation is much smaller and can be characterized by average values. Thus, the task reduces to determining the ratio of the average nighttime to daytime concentration, $r_i = n_i^n/n_i^d$, which is found by appropriately simplifying the time-dependent photochemical equation (without diffusion). The parameters r_i are used to modify the photolysis and gas kinetic rates by taking a 24-hour average of the chemical terms in the conservation equation. For a bimolecular reaction between species i and j, a typical chemical term can be written as

$$kn_in_j \tag{25}$$

and its 24-hour average is

$$k \frac{1}{t_o} \int_0^{t_o} n_in_j \, dt \approx k\left(\frac{t^d}{t_o} n_i^d n_j^d + \frac{t^n}{t_o} n_i^n n_j^n\right) \tag{26}$$

where $t_o = 24$ hours and t^d and t^n represent the length of the day and night. However, n_i^n is related to n_i^d through the quantity r_i, so that equation (26) reduces to

$$kn_i^d n_j^d\left(\frac{t^d}{t_o} + r_ir_j \frac{t^n}{t_o}\right) \tag{27}$$

The quantity n_i^d can be expressed in terms of the 24-hour average $\bar{n}_i$ as follows:

$$\bar{n}_i = \frac{1}{t_o} \int_0^{t_o} n_i \, dt = \frac{t^d}{t_o} n_i^d + \frac{t^n}{t_o} n_i^n = n_i^d\left(\frac{t^d}{t_o} + r_i \frac{t^n}{t_o}\right)$$

$$= \delta_i n_i^d \tag{28}$$

Use of this last expression in equation (27) gives

$$\frac{k\left(\frac{t^d}{t_o} + r_ir_j \frac{t^n}{t_o}\right)}{\delta_i\delta_j} \bar{n}_i\bar{n}_j = \tilde{k}\bar{n}_i\bar{n}_j \tag{29}$$

15

which has the same form as equation (25). For a term involving photolysis, the 24-hour average is

$$\frac{1}{t_o} \int_0^{t_o} J_i n_i \, dt \approx \frac{t_d}{t_o} J_i{}^d n_i{}^d = \frac{\bar{J}_i}{\delta_i} \bar{n}_i \tag{30}$$

where it is assumed that the photolysis rate is constant over the day at its daytime average. The last term in equation (30) is obtained by noting that $\bar{J}_i$, the 24-hour average photolysis rate, is related to its daytime average according to $\bar{J}_i = \dfrac{t_d}{t_o} J_i{}^d$ and by using equation (28). Values of $\bar{J}_i$ were calculated by a procedure analogous to that employed in reference 19. This method allows for the variation of solar zenith angle over the day rather than evaluating the photolysis rate at some mean zenith angle.

As the derivation outlined in the previous paragraph illustrates, the key quantity for including diurnal effects in a constant sun model is the parameter r_i. For many species, this parameter can be determined immediately. Species with long chemical lifetimes, such as CH_4, N_2O, Freons, CO, HCl, HNO_3, and O_3, have little diurnal variation so that $r_i = 1$ is a good approximation. On the other hand, species with very short chemical lifetimes, such as O and NO, decrease rapidly at sunset to essentially zero at night so that $r_i \approx 0$. For species with intermediate lifetimes, r_i must be calculated by suitably simplifying the photochemical equations for nighttime chemistry. In the present work, this procedure is used to obtain explicit expressions for r_i for NO_2, NO_3, N_2O_5, $ClONO_2$, ClO, and HO_2. All other species are assumed to have a value of r_i equal to either 0 or 1 depending on their reactivity. It should be noted that a species may exhibit some dirunal variation, which implies that r_i is near unity, but because it is relatively unimportant in the chemistry, the simpler procedure of ignoring its variation is adopted. In order to illustrate the type of manipulations required, the derivation of r_i for $ClONO_2$ is given in detail in the appendix. A summary of the results for all of the species, along with basic assumptions made in the derivations, is also given in the appendix.

INPUT DATA

Transport

The eddy diffusion coefficient used in the present calculations is plotted in figure 3 along with others used recently in various models. The current choice of the K_z function for this model is that recommended in reference 17. At the present time, it is difficult to state what the most appropriate K_z profile is for one-dimensional calculations. At best, K_z must be regarded as a transport parameter determined, insofar as possible, by available tracer or vertical mixing data.

16

Photochemical Data

The kinetic mechanism considered in the model includes 115 reactions involving 36 active species. The specific reactions and rate data employed are listed in table I, along with the data sources from which they were obtained. (See refs. 4, 12, 17, and 20 to 44.) Solar intensity data at the outer edge of the atmosphere were taken from reference 12, with the modifications to the ultraviolet wavelengths indicated in reference 13. The photolysis rates shown in table I(b) are noontime values at 55 km for a 45° solar zenith angle. Molecular oxygen number densities are held fixed and are taken from reference 10. It must be recognized that large uncertainties remain in many of the rate coefficients, and the possibility exists that important processes and species remain to be discovered. Thus, current sets of reactions and species are subject to periodic review and alteration.

Loss Rates for Condensible and Soluble Species

To represent in a reasonable way the globally averaged vertical concentration profiles of condensible and soluble species in the troposphere, it is necessary to account for precipitation removal processes. Of course, the most important species in this category for the Earth's atmosphere is H_2O, and the use of its precipitation factor in this model is presented in some detail. Below the tropopause, precipitation processes are primarily responsible for the average lifetime of a water vapor molecule in the atmosphere. As a first approximation in determining a value for this lifetime, a continuity equation for water vapor is written:

$$\frac{\partial n_{H_2O}}{\partial t} = -\frac{\partial \Phi_{H_2O}}{\partial z} - \frac{n_{H_2O}}{q_{H_2O}} \tag{31}$$

where q_{H_2O} is the precipitation lifetime of H_2O and the last term represents a loss rate of water vapor due entirely to the condensation and subsequent rainout processes. Production and loss due to chemical reactions are negligible. Using the vertical eddy diffusion coefficient defined previously and assuming steady state, this equation becomes

$$-\frac{d}{dz}\left[-nK_z\frac{d}{dz}\left(\frac{n_{H_2O}}{n}\right)\right] - \frac{n_{H_2O}}{q_{H_2O}} = 0 \tag{32}$$

where n is the total number density. Since the water vapor mole fraction may be defined as

17

$$\chi_{H_2O} = \frac{n_{H_2O}}{n} \tag{33}$$

equation (32) may be rewritten as

$$\frac{d^2\chi_{H_2O}}{dz^2} + \frac{d(\ln\ n)}{dz} \frac{d\chi_{H_2O}}{dz} - \frac{\chi_{H_2O}}{K_z q_{H_2O}} = 0 \tag{34}$$

This equation may be used to determine reasonable values of q_{H_2O} for use in one-dimensional models if χ_{H_2O}, n, and K_z are known functions of altitude. With values of n and χ_{H_2O} from reference 45 and values of K_z cited previously, the inverse lifetime, deduced from a numerical solution of equation (34), is found to be closely represented by

$$\frac{1}{q_{H_2O}} = K_z(0.076z + 0.25)^2 \tag{35}$$

where K_z is in m^2-s^{-1} and z is in km. Since water vapor is relatively unreactive in the troposphere, this analysis should yield a value of q_{H_2O} which gives reasonable results in a coupled chemistry model. Specifically, for ambient conditions, the global average tropospheric water vapor profile from which the lifetime expression is derived should be essentially reproduced. When studies are performed involving water vapor injections at various altitudes, the present formulation provides a means of investigating resultant water vapor production, loss, and altered concentration profile in a self-consistent manner within the model. The inclusion of the lifetime expression in the model is simply accomplished by adding the term n_{H_2O}/q_{H_2O} to the chemical loss term $L_{H_2O}n_{H_2O}$. Figure 4 shows the tropospheric water vapor profile for the unperturbed atmosphere calculated with the model, along with profiles obtained from other sources. It is apparent that the present calculation represents what may be reasonably considered a globally averaged vertical distribution.

A very rough estimate of the water vapor lifetime may be obtained by dividing the average atmospheric water vapor content by the mean precipitation rate. The total water vapor content may be easily approximated by

18

integration of a mole fraction profile represented by a 2-km scale height distribution. (This profile is also shown in fig. 4.) Such a calculation leads to a value of 2.67×10^{43} H_2O molecules in the atmosphere. Reference 46 gives the annual precipitation rate as 200.9 cm-year^{-1}, which converts to 1.09×10^{38} molecules-s^{-1}. The average lifetime based on these two values is 2.83 days. The tropospheric lifetime q_{H_2O} obtained from equation (35) varies

with altitude between values of about 1 to 18 days. Thus, an average lifetime as represented in equation (35) is reasonably similar in magnitude to the value based on data sources. However, it is impossible to state exactly what the global mean lifetime of H_2O actually is without access to more accurate and widespread data on global precipitation. As is stated in reference 47, the atmosphere holds on the average about 10 days' supply of water, but, in heavy rainfall areas, the columnar H_2O content demands a moisture supply which corresponds to a lifetime of only 1 or 2 hours.

In addition to water vapor, the soluble species for which rainout factors are included in the troposphere are HCl, HNO_3, and CH_3OOH. Of course, for these trace constituents, an estimate of rainout lifetime as described previously for water vapor is not possible because of their relative chemical activity in the troposphere and a lack of sufficiently extensive global data on their average vertical concentration profiles. For these reasons, the rainout factors presently used for these species are rough estimates. A constant value of inverse rainout lifetime of 3×10^{-6} s^{-1} is used for both HNO_3 and HCl (ref. 48) for $0 < z < 9$ km, while the precipitation factor for CH_3OOH is equated to that of H_2O. More rigorous approaches to the problem of soluble gases in the atmosphere may be found, for example, in reference 49.

Radiation Data

Figure 5 summarizes the solar and infrared bands of O_3, H_2O, and CO_2 treated in the radiative transfer model. Band absorptance and emissivity expressions, along with required input data such as bandwidths and strengths and line half-widths, are taken from reference 8.

Boundary Conditions

In addition to the chemical and radiative input data described previously, conditions at the upper and lower boundaries of the calculations are of utmost importance in this type of solution; and for some of the minor atmospheric constituents, specification of appropriate boundary conditions is difficult. In this model, three types of boundary conditions may be used: fixed number density, fixed particle flux, and photochemical equilibrium. The boundary conditions imposed on each of the species at 0 and 55 km for the present calculation are given in table II. When chemical lifetimes are relatively short (on the order of minutes), equilibrium conditions are used, and when number densities have been well established, these values are selected. The specification of zero flux for a species means that the volume concentration, or mole fraction, of that species is constant across the boundary.

SAMPLE CALCULATIONS

Using the input data and boundary conditions just described, some results of a temperature-coupled solution of the current model are presented. Although these results are for a nominal ambient atmosphere, the model is capable of including chlorofluoromethanes (CF_2Cl_2 and $CFCl_3$) and their by-products in the calculations. Figure 6 shows the vertical concentration profiles of the various species for the converged steady-state solution. The discontinuity in the K_z parameter at 14.5 km (see fig. 3) results in slope discontinuities in several of the species profiles. The cloud cover parameters at 5 km result in similar behavior. These profiles have been found in general to compare favorably with other computations and experimental data distributions. Figure 7 compares the temperature profile calculated by the model with the profile of reference 10. The temperature deviations in the lower stratosphere are characteristic of one-dimensional radiative-convective calculations (see for example, ref. 8) and are due to dynamical effects which are not taken into account in the model.

The program output includes printed values of number densities and/or mole fractions for all species at each altitude node point as well as the temperature structure. Optional printout and plotting is available for the production and loss of each species due to each reaction. Curves of this sort for the various species are extremely helpful in analysis of the solution, for example, in determining which processes are significant at various altitudes.

CONCLUDING REMARKS

A computational one-dimensional model of the Earth's atmosphere has been discussed and some of the more salient and unique features have been described in detail. In addition, input data based on the most recent available information have been presented, along with results obtained using these data. This model, along with several others in current use, gives a reasonable representation of many aspects of the globally averaged atmosphere and should continue to be useful in future studies of processes which impact the physical and chemical state of the atmosphere. Of course, of primary concern are those perturbations which impact the ozone layer in the stratosphere and the overall thermal balance of the planet.

It must be recognized that a one-dimensional model, however refined, is only a first approximation to the actual globally averaged atmosphere. Nevertheless, it is encouraging that this and similar models depict many important chemical and thermal properties in satisfactory agreement with observations. Because of this feature, their relative simplicity and their computational economy, one-dimensional models will have continued usefulness in a variety of applications, such as parametric and sensitivity studies of various chemical schemes and initial assessments of man-induced perturbations of the physical state of the atmosphere.

Langley Research Center
National Aeronautics and Space Administration
Hampton, VA 23665
February 12, 1979

APPENDIX

DERIVATION OF DIURNAL PARAMETERS FOR $ClONO_2$,

ClO, HO_2, NO_2, N_2O_5, AND NO_3

For the Langley model, the six species $ClONO_2$, ClO, HO_2, NO_2, N_2O_5, and NO_3 are the only ones considered for special values of the diurnal parameter r_i. The other species are assumed to have either no diurnal variation or to be present only during the presence of sunlight. In the latter category are NO, O, OH, H, $O(^1D)$, N, ClO_2, CH_3, HCO, and CH_3O. Those species which are assumed not to vary between day and night are O_3, HNO_3, HNO_2, H_2O_2, N_2O, H_2O, HCl, Cl_2, CF_2Cl_2, $CFCl_3$, CH_4, CO, CCl_4, CH_3Cl, CH_2O, and CH_3OOH. The output of the calculations can be formulated to give either daytime concentrations and/or the average 24-hour concentrations.

In this appendix the diurnal parameter for $ClONO_2$ is derived, and the derivations of r_i for the other five species are summarized. The diurnal parameters derived pertain specifically to the set of reactions listed in table I. Inclusion of additional species or changes in the rate constants will require a reevaluation of these parameters because the relative ordering of the photochemical terms retained may be changed. The procedures outlined in this appendix, however, remain unchanged.

Derivation of Diurnal Parameters for $ClONO_2$ and ClO

The only significant nighttime chemistry for $ClONO_2$ involves its formation due to the reaction between ClO and NO_2, so that its time variation during the night can be written approximately as

$$\frac{d[ClONO_2]}{dt} \approx k_{67}[NO_2]^n[M][ClO] = P^n[ClO] \tag{A1}$$

while during the day, its variation is approximately

$$\frac{d[ClONO_2]}{dt} = P^d[ClO] - L^d[ClONO_2] \tag{A2}$$

where

$$\left.\begin{aligned} P^d &= k_{67}[NO_2]^d[M] \\ L^d &= J_{21}^d + k_{69}[O]^d \end{aligned}\right\} \tag{A3}$$

and the superscripts d and n signify daytime and nighttime averages. In order to solve these equations, it is necessary to relate the concentration of ClO to that of $ClONO_2$. This relationship is obtained by noting that the total Cl family concentration, $[Cl_x]$, which includes all species containing chlorine other than the source molecules (Freons, CCl_4, and CH_3Cl), is long-lived and has no appreciable diurnal variation. Thus, over 24 hours

$$[Cl_x] = [Cl] + [ClO] + [ClOO] + 2[Cl_2] + [HCl] + [ClONO_2] \qquad (A4)$$

is essentially constant. Although the Cl_2 concentration increases at night, its contribution to the family sum is a few percent at most, so that its variation is neglected and its concentration is set equal to its daytime average value. Furthermore, exact time-dependent calculations (ref. 16) show that HCl has no significant diurnal variation (i.e., $r_{HCl} = 1$). Use of these last two assumptions in conjunction with equation (A4) allow one to write

$$\left[\overline{Cl_x}\right] = [Cl] + [ClO] + [ClOO] + [ClONO_2] \qquad (A5)$$

$$= Constant$$

Equation (A5) is further simplified by assuming that [ClO], [Cl], and [ClOO] rapidly equilibrate. Thus, during the day, equation (A5) reduces to

$$\left[\overline{Cl_x}\right]^d = [ClO]G + [ClONO_2] \qquad (A6)$$

where

$$G = 1 + f$$

$$f = f_1(1 + f_2)$$

$$f_1 = \frac{k_{45}[O]^d + k_{46}[NO]^d}{k_{44}[O_3]}$$

$$f_2 = \frac{k_{55}[O_2]}{k_{56}}$$

At sunset, [Cl] and [ClOO] go very rapidly to zero while [ClO] changes more slowly, so that for a few hours after sunset,

$$\left[\overline{Cl_x}\right]^n \approx [ClO] + [ClONO_2] \qquad (A7)$$

APPENDIX

Equations (A1) and (A2) can now be solved using equations (A6) and (A7) and the constraint that $[ClONO_2]$ at time $t + 24$ equals its value at time t. The resulting expressions can be integrated to obtain daytime and nighttime average concentrations. After much algebraic manipulation, the final results are

$$\frac{[ClONO_2]^d}{[\overline{Cl_x}]} = \frac{\dfrac{P^d}{G} + F_1 L^d}{L^T} \tag{A8}$$

$$\frac{[ClONO_2]^n}{[\overline{Cl_x}]} = 1 - \frac{L^d}{L^T} F_2 \tag{A9}$$

where

$$L^T = \frac{P^d}{G} + L^d$$

$$F_1 = \frac{[1 - \exp(-P^n T^n)][1 - \exp(-L^T T^d)]}{L^T T^d\{1 - \exp[-(L^T T^d + P^n T^n)]\}}$$

$$F_2 = \frac{L^T T^d}{P^n T^n} F_1$$

Daytime and nighttime average concentrations of ClO can be expressed in terms of those for $ClONO_2$ by using equations (A6) and (A7) as follows:

$$\frac{[ClO]^d}{[\overline{Cl_x}]} = \frac{1}{G}\left(1 - \frac{[ClONO_2]^d}{[\overline{Cl_x}]}\right) \tag{A10}$$

$$\frac{[ClO]^n}{[\overline{Cl_x}]} = 1 - \frac{[ClONO_2]^n}{[\overline{Cl_x}]} \tag{A11}$$

The ratios of equations (A9) with (A8) and (A11) with (A10) give the values of r_i for $ClONO_2$ and ClO, respectively.

Derived Diurnal Parameters for Other Species

$\underline{NO_2}$.- For this species, it is assumed that the daytime value of $[NO] + [NO_2]$ is equivalent to the nighttime value of $[NO_2]$ (see ref. 16); thus,

$$r_{NO_2} = \frac{[NO_2]^n}{[NO_2]^d} = \frac{[NO]^d + [NO_2]^d}{[NO_2]^d} = 1 + \frac{[NO]^d}{[NO_2]^d} \tag{A12}$$

Using the dominant production and loss terms in a chemical equilibrium expression for $[NO_2]$ gives

$$\frac{[NO]^d}{[NO_2]^d} = \frac{J_4^d + k_8[O]^d}{k_{13}[O_3]^d + k_{20}[HO_2]^d + k_{46}[ClO]^d} \tag{A13}$$

which may be substituted directly into equation (A12).

$\underline{HO_2}$.- To obtain the diurnal parameter for this species, it is assumed that, during daylight, photochemical equilibrium conditions exist. During the night, retention of the dominant chemical terms yields the following rate expression:

$$\frac{d[HO_2]}{dt} = -L^n[HO_2] - 2k_{22}[HO_2]^2 \tag{A14}$$

where

$$L^n = k_{28}[O_3] + k_{70}[NO_2]^n$$

Equation (A14) may be integrated over the nighttime t^n and an average nighttime concentration obtained:

$$[HO_2]^n = \frac{1}{2k_{22}t^n} \ln\left\{1 + \frac{2k_{22}[HO_2]^d}{L^n}[1 - \exp(-L^n t^n)]\right\}$$

$$\approx \frac{[HO_2]^d}{L^n t^n}[1 - \exp(-L^n t^n)] \tag{A15}$$

This last approximation is valid because

$$\frac{2k_{22}[HO_2]^d}{L^n} \ll 1$$

Thus,

$$r_{HO_2} = \frac{1}{L^n t^n}[1 - \exp(-L^n t^n)] \tag{A16}$$

$\underline{N_2O_5}$.- Two differential equations for rate of change of N_2O_5 (a daytime equation and a nighttime equation) are solved by using the dominant production and loss terms. During sunlight hours,

$$\frac{d[N_2O_5]}{dt} \approx -\left(J_{13}^d + k_{36}[M] + k_{38}[O]^d\right)[N_2O_5] \tag{A17}$$

During nighttime (assuming chemical equilibrium for $[NO_3]$),

$$\frac{d[N_2O_5]}{dt} \approx k_{14}[NO_2]^n[O_3] \tag{A18}$$

When equation (A17) is integrated over daytime and equation (A18) over nighttime and the constraint of cyclic variation is imposed, the following expressions are obtained:

$$[N_2O_5]^d = \frac{k_{14}[NO_2]^n[O_3]t^n}{L^d t^d} \tag{A19}$$

$$[N_2O_5]^n = \frac{1}{2} k_{14}[NO_2]^n[O_3]t^n \left[\frac{1 + \exp(-L^d t^d)}{1 - \exp(-L^d t^d)}\right] \tag{A20}$$

Thus,

$$r_{N_2O_5} = \frac{L^d t^d}{2} \left[\frac{1 + \exp(-L^d t^d)}{1 - \exp(-L^d t^d)} \right] \tag{A21}$$

where

$$L^d = J_{13}^d + k_{36}[M] + k_{38}[O]^d$$

$\underline{NO_3}$.- For the diurnal parameter of NO_3, chemical equilibrium is invoked for both conditions. In the absence of sunlight,

$$[NO_3]^n \approx \frac{k_{36}[N_2O_5]^n[M] + k_{14}[NO_2]^n[O_3]}{k_{35}[NO_2]^n[M]} \tag{A22}$$

The daytime expression is more complex:

$$[NO_3]^d = \frac{P_{NO_3}^d}{L_{NO_3}^d} \tag{A23}$$

where

$$P_{NO_3}^d = J_{13}^d[N_2O_5]^d + k_{69}[O]^d[ClONO_2]^d + k_{51}[Cl]^d[HNO_3]$$

$$+ k_{36}[M][N_2O_5]^d + k_{34}[NO_2]^d[O]^d[M] + k_{29}[OH]^d[HNO_3]$$

$$+ k_{14}[O_3][NO_2]^d + k_9[O]^d[HNO_3]$$

and

$$L_{NO_3}^d = J_{11}^d + J_{10}^d + k_{35}[NO_2]^d[M] + k_{23}[NO]^d$$

As before, the ratio of equations (A22) to (A23) gives the value of r_{NO_3}.

REFERENCES

1. Boughner, R. E.: The Effect of Increased Carbon Dioxide Concentrations on Stratospheric Ozone. J. Geophys. Res., vol. 83, no. C3, Mar. 20, 1978, pp. 1326-1332.

2. Nealy, J. E.; Callis, L. B.; and Natarajan, M.: Effects of Solar Cycle UV Radiance Variations on Stratospheric Structure. EΘS, Trans., American Geophys. Union, vol. 58, no. 12, Dec. 1977, p. 1200.

3. Callis, L. B.; and Nealy, J. E.: Solar UV Variability and Its Effect on Stratospheric Thermal Structure and Trace Constituents. Geophys. Res. Lett., vol. 5, no. 4, Apr. 1978, pp. 249-252.

4. Wofsy, Steven C.; McConnell, John C.; and McElroy, Michael B.: Atmospheric CH_4, CO, and CO_2. J. Geophys. Res., vol. 77, no. 24, Aug. 20, 1972, pp. 4477-4493.

5. Stewart, Richard W.; and Hoffert, Martin I.: A Chemical Model of the Troposphere and Stratosphere. J. Atmos. Sci., vol. 32, no. 1, Jan. 1975, pp. 195-210.

6. Shimazaki, T.; and Whitten, R. C.: A Comparison of One-Dimensional Theoretical Models of Stratospheric Minor Constituents. Rev. Geophys. & Space Phys., vol. 14, no. 1, Feb. 1976, pp. 1-12.

7. Turco, R. P.; and Whitten, R. C.: The NASA Ames Research Center One- and Two-Dimensional Stratospheric Models - Part I: The One-Dimensional Model. NASA TP-1002, 1977.

8. Ramanathan, V.: Radiative Transfer Within the Earth's Troposphere and Stratosphere: A Simplified Radiative-Convective Model. J. Atmos. Sci., vol. 33, no. 7, July 1976, pp. 1330-1346.

9. Fox, L.: An Introduction to Numerical Linear Algebra. Oxford Univ. Press, 1965.

10. U.S. Standard Atmosphere, NASA, U.S. Air Force, and U.S. Weather Bur., Dec. 1962.

11. McClatchey, R. A.; Fenn, R. W.; Selby, J. E. A.; Volz, F. E.; and Garing, J. S.: Optical Properties of the Atmosphere (Third Edition), AFCRL-72-0497, U.S. Air Force, Aug. 24, 1972. (Available from DDC as AD 753 075.)

12. Ackerman, M.: Ultraviolet Solar Radiation Related to Mesospheric Processes. Mesospheric Models and Related Experiments, G. Fiocco, ed., Springer-Verlag New York, Inc., c.1971, pp. 149-159.

13. Simon, P.: Balloon Measurements of Solar Fluxes Between 1960 Å and 2300 Å. Proceedings of the Third Conference on the Climatic Impact Assessment Program, Anthony J. Broderick and Thomas M. Hard, eds. DOT-TSC-OST-74-15, U.S. Dep. Transp., Nov. 1974, pp. 137-142.

14. Penndorf, Rudolf: Tables of the Refractive Index for Standard Air and the Rayleigh Scattering Coefficient for the Spectral Region Between 0.2 and 20.0 μ and Their Application to Atmospheric Optics. J. Opt. Soc. America, vol. 47, no. 2, Feb. 1957, pp. 176-182.

15. Callis, Linwood B.: The Radiative Transfer Equation and Environmental Effects in the Upper Atmosphere. AIAA Paper 72-663, 1972.

16. Kurzeja, Robert J.: The Diurnal Variation of Minor Constituents in the Stratosphere and Its Effect on the Ozone Concentration. J. Atmos. Sci., vol. 32, no. 5, May 1975, pp. 899-909.

17. Hudson, Robert D., ed.: Chlorofluoromethanes and the Stratosphere. NASA RP-1010, 1977.

18. Turco, R. P.; and Whitten, R. C.: A Note on the Diurnal Averaging of Aeronomical Models. J. Atmos. & Terrest. Phys., vol. 40, no. 1, Jan. 1978, pp. 13-20.

19. Rundel, R. D.: Determination of Diurnal Average Photodissociation Rates. J. Atmos. Sci., vol. 34, no. 4, Apr. 1977, pp. 639-641.

20. Hampson, Robert F., Jr.; and Garvin, David, eds.: Reaction Rate and Photochemical Data for Atmospheric Chemistry - 1977. NBS Spec. Publ. 513, U.S. Dep. Commer., May 1978.

21. Watson, R. T.: Rate Constants for Reactions of ClO_x of Atmospheric Interest. J. Phys. Chem. Ref. Data, vol. 6, no. 3, 1977, pp. 871-917.

22. Simonaitis, R.; and Heicklen, Julian: Reactions of CH_3O_2 With NO and NO_2. J. Phys. Chem., vol. 78, no. 24, Nov. 21, 1974, pp. 2417-2421.

23. Perry, R. A.; Atkinson, R.; and Pitts, J. N., Jr.: Kinetics of the Reactions of OH Radicals With C_2H_2 and CO. J. Chem. Phys., vol. 67, no. 12, Dec. 15, 1977, pp. 5577-5584.

24. Hudson, Robert D.; and Mahle, Stephen H.: Interpolation Constants for Calculation of Transmittance and Rate of Dissociation of Molecular Oxygen in the Mesosphere and Lower Thermosphere. NASA TM X-58084, 1972.

25. Hasson, V.; and Nicholls, R. W.: Absolute Spectral Absorption Measurements on Molecular Oxygen From 2640-1920 Å: II. Continuum Measurements 2430-1920 Å. J. Phys. B, Atomic & Mol. Phys., vol. 4, 1971, pp. 1789-1797.

26. Moortgat, Geert Karel; and Kudszus, Eberhard: Mathematical Expression for the $O(^1D)$ Quantum Yields From the O_3 Photolysis as a Function of Temperature (230–320 K) and Wavelength (295–320 nm). Geophys. Res. Lett., vol. 5, no. 3, Mar. 1978, pp. 191–194.

27. Sullivan, J. O.; and Holland, A. C.: A Congeries of Absorption Cross Sections for Wavelengths Less Than 3000 Å. NASA CR-371, 1966.

28. Hall, T. C., Jr.; and Blacet, F. E.: Separation of the Absorption Spectra of NO_2 and N_2O_4 is the Range of 2400–5000 Å. J. Chem. Phys., vol. 20, no. 11, Nov. 1952, pp. 1745–1749.

29. Johnston, Harold S.; and Graham, Richard: Photochemistry of NO_x and HNO_x Compounds. Canadian J. Chem., vol. 52, no. 8 (pt. 2), Apr. 15, 1974, pp. 1415–1423.

30. Molina, Luisa T.; Schinke, Stanley D.; and Molina, Mario J.: Ultraviolet Absorption Spectrum of Hydrogen Peroxide Vapor. Geophys. Res. Lett., vol. 4, no. 12, Dec. 1977, pp. 580–582.

31. Holt, R. B.; McLane, C. K.; and Oldenberg, O.: Ultraviolet Absorption Spectrum of Hydrogen Peroxide. J. Chem. Phys., vol. 16, no. 3, Mar. 1948, pp. 225–229.

32. Bates, D. R.; and Hays, P. B.: Atmospheric Nitrous Oxide. Planet. & Space Sci., vol. 15, no. 1, Jan. 1967, pp. 189–197.

33. Zelikoff, Murray; Watanabe, K.; and Inn, Edward C. Y.: Absorption Coefficients of Gases in the Vacuum Ultraviolet. Part II. Nitrous Oxide. J. Chem. Phys., vol. 21, no. 10, Oct. 1953, pp. 1643–1647.

34. Johnston, H. S.; and Selwyn, G. S.: New Cross Sections for the Absorption of Near Ultraviolet Radiation by Nitrous Oxide (N_2O). Geophys. Res. Lett., vol. 2, no. 12, Dec. 1975, pp. 549–551.

35. Cieslik, S.; and Nicolet, M.: The Aeronomic Dissociation of Nitric Oxide. Planet. & Space Sci., vol. 21, no. 6, June 1973, pp. 925–938.

36. Inn, Edward C. Y.: Absorption Coefficient of HCl in the Region 1400 to 2200 Å. J. Atmos. Sci., vol. 32, no. 12, Dec. 1975, pp. 2375–2377.

37. Watson, R. T.: Chemical Kinetics Data Survey VIII. Rate Constants of ClO_x of Atmospheric Interest. NBSIR 74-516, U.S. Dep. Commer., June 1974.

38. Bresler, P. I.; and Shtilerman, G. A.: Absorption Coefficients of Chlorine and Fluorine in the 220–470 nm Range. J. Appl. Spectros., vol. 14, no. 4, Apr. 1971 (Sept. 15, 1973), pp. 538–539.

39. Chou, C. C.; Smith, W. S.; Ruiz, H. Vera; Moe, K.; Crescentini, G.; Molina, M. J.; and Rowland, F. S.: The Temperature Dependences of the Ultraviolet Absorption Cross Sections of CCl_2F_2 and CCl_3F, and Their Stratospheric Significance. J. Phys. Chem., vol. 81, no. 4, Feb. 24, 1977, pp. 286-290.

40. Rowland, F. S.; Spencer, John E.; and Molina, Mario J.: Stratospheric Formation and Photolysis of Chlorine Nitrate. J. Phys. Chem., vol. 80, no. 24, Nov. 18, 1976, pp. 2711-2713.

41. Rowland, F. S.; and Molina, Mario J.: Chlorofluoromethanes in the Environment. Rev. Geophys. & Space Phys., vol. 13, no. 1, Feb. 1975, pp. 1-35.

42. Robbins, Donald E.: Photodissociation of Methyl Chloride and Methyl Bromide in the Atmosphere. Geophys. Res. Lett., vol. 3, no. 4, Apr. 1976, pp. 213-216.

43. Calvert, Jack G.; Kerr, J. Alistair; Demerjian, Kenneth L.; and McQuigg, Robert D.: Photolysis of Formaldehyde as a Hydrogen Atom Source in the Lower Atmosphere. Science, vol. 175, no. 4023, Feb. 18, 1972, pp. 751-752.

44. Chameides, W. L.; and Stedman, D. H.: Tropospheric Ozone: Coupling Transport and Photochemistry. J. Geophys. Res., vol. 82, no. 12, Apr. 20, 1977, pp. 1787-1794.

45. U.S. Standard Atmosphere Supplements, 1966. Environ. Sci. Serv. Admin., NASA, and U.S. Air Force.

46. Palmén, E.; and Newton, C. W.: Atmospheric Circulation Systems - Their Structure and Physical Interpretation. Academic Press, Inc., 1969.

47. Lamb, H. H.: Climate: Present, Past and Future. Volume 1 - Fundamentals and Climate Now. Methuen & Co., Ltd. (London), c.1972.

48. Wofsy, Steven C.; McElroy, Michael B.; and Sze, Nien Dak: Freon Consumption: Implications for Atmospheric Ozone. Science, vol. 187, no. 4176, Feb. 14, 1975, pp. 535-536.

49. Stedman, D. H.; Chameides, W. L.; and Cicerone, R. J.: The Vertical Distribution of Soluble Gases in the Atmosphere. Geophys. Res. Lett., vol. 2, no. 8, Aug. 1975, pp. 333-336.

TABLE I.- PHOTOCHEMICAL PROCESSES FOR LANGLEY ONE-DIMENSIONAL MODEL

(a) Kinetic process

Process	Rate expression (a)	Ref.
(1) $O(^1D) + O_2 \rightarrow O + O_2$	$2.9 \times 10^{-11} \exp(67/T)$	20
(2) $O(^1D) + N_2 \rightarrow O + N_2$	$2.0 \times 10^{-11} \exp(107/T)$	20
(3) $O(^1D) + H_2O \rightarrow 2OH$	2.3×10^{-10}	20
(4) $O + O_2 + M \rightarrow O_3 + M$	$1.07 \times 10^{-34} \exp(510/T)$	20
(5) $O + O_3 \rightarrow 2O_2$	$1.9 \times 10^{-11} \exp(-2300/T)$	20
(6) $O + OH \rightarrow H + O_2$	4.2×10^{-11}	20
(7) $O + HO_2 \rightarrow OH + O_2$	3.5×10^{-11}	20
(8) $O + NO_2 \rightarrow NO + O_2$	9.1×10^{-12}	20
(9) $O + HNO_3 \rightarrow NO_3 + OH$	2.0×10^{-17}	20
(10) $O + HNO_2 \rightarrow NO_2 + OH$	3.0×10^{-17}	20
(11) $O_2 + H + M \rightarrow HO_2 + M$	$2.08 \times 10^{-32} \exp(290/T)$	20
(12) $O_3 + OH \rightarrow HO_2 + O_2$	$1.5 \times 10^{-12} \exp(-1000/T)$	20
(13) $O_3 + NO \rightarrow NO_2 + O_2$	$2.1 \times 10^{-12} \exp(-1450/T)$	20
(14) $O_3 + NO_2 \rightarrow NO_3 + O_2$	$1.2 \times 10^{-13} \exp(-2450/T)$	20
(15) $O_3 + H \rightarrow OH + O_2$	$1.0 \times 10^{-10} \exp(-516/T)$	20
(16) $2OH \rightarrow H_2O + O$	$1.0 \times 10^{-11} \exp(-550/T)$	20
(17) $OH + HO_2 \rightarrow H_2O + O_2$	3.0×10^{-11}	20
(18) $OH + NO_2 + M \rightarrow HNO_3 + M$	[b]$0.94 \, \phi_1([M],T)$	20
(19) $OH + NO + M \rightarrow HNO_2 + M$	$0.25k_{18}$	(c)
(20) $HO_2 + NO \rightarrow OH + NO_2$	8.1×10^{-12}	20
(21) $OH + H_2O_2 \rightarrow H_2O + HO_2$	$1.0 \times 10^{-11} \exp(-750/T)$	20
(22) $2HO_2 \rightarrow H_2O_2 + O_2$	2.5×10^{-12}	20
(23) $NO + NO_3 \rightarrow 2NO_2$	1.9×10^{-11}	20
(24) $NO + O + M \rightarrow NO_2 + M$	$1.55 \times 10^{-32} \exp(584/T)$	20
(25) $N_2O + O(^1D) \rightarrow N_2 + O_2$	5.5×10^{-11}	20
(26) $N_2O + O(^1D) \rightarrow 2NO$	5.5×10^{-11}	20
(27) $O(^1D) + N_2 + M \rightarrow N_2O + M$	3.5×10^{-37}	20
(28) $HO_2 + O_3 \rightarrow OH + 2O_2$	$7.3 \times 10^{-14} \exp(-1275/T)$	20
(29) $OH + HNO_3 \rightarrow H_2O + NO_3$	8.0×10^{-14}	20
(30) $O(^1D) + H_2 \rightarrow OH + H$	9.9×10^{-11}	20
(31) $OH + HNO_2 \rightarrow H_2O + NO_2$	6.6×10^{-12}	20
(32) $O(^1D) + CH_4 \rightarrow OH + CH_3$	1.3×10^{-10}	20
(33) $NO + HO_2 + M \rightarrow HNO_3 + M$	$1.0 \times 10^{-15}/[M]$	20
(34) $NO_2 + O + M \rightarrow NO_3 + M$	1.0×10^{-31}	20
(35) $NO_2 + NO_3 + M \rightarrow N_2O_5 + M$	[d]$\phi_3([M],T)$	20
(36) $N_2O_5 + M \rightarrow NO_2 + NO_3 + M$	[e]$\phi_4([M],T)$	20
(37) $N_2O_5 + H_2O \rightarrow 2HNO_3$	1.0×10^{-20}	20
(38) $N_2O_5 + O \rightarrow 2NO_2 + O_2$	1.0×10^{-14}	20
(39) $N + NO_2 \rightarrow N_2O + O$	$2.0 \times 10^{-11} \exp(-800/T)$	20
(40) $N + O_2 \rightarrow NO + O$	$5.5 \times 10^{-12} \exp(-3200/T)$	20

See footnotes at end of table, page 33.

TABLE I.- Continued

(a) Continued

	Process	Rate expression (a)	Ref.
(41)	$N + NO \rightarrow N_2 + O$	$8.2 \times 10^{-11} \exp(-410/T)$	20
(42)	$N + NO_2 \rightarrow 2NO$	0	20
(43)	$N + O_3 \rightarrow NO + O_2$	$2.0 \times 10^{-11} \exp(-1070/T)$	20
(44)	$Cl + O_3 \rightarrow ClO + O_2$	$2.7 \times 10^{-11} \exp(-257/T)$	20
(45)	$ClO + O \rightarrow Cl + O_2$	$7.7 \times 10^{-11} \exp(-130/T)$	20
(46)	$ClO + NO \rightarrow Cl + NO_2$	$1.0 \times 10^{-11} \exp(200/T)$	20
(47)	$Cl + CH_4 \rightarrow HCl + CH_3$	$7.3 \times 10^{-12} \exp(-1269/T)$	20
(48)	$Cl + H_2 \rightarrow HCl + H$	$3.5 \times 10^{-11} \exp(-2290/T)$	20
(49)	$Cl + HO_2 \rightarrow HCl + O_2$	3.0×10^{-11}	20
(50)	$Cl + H_2O_2 \rightarrow HCl + HO_2$	$1.7 \times 10^{-12} \exp(-384/T)$	20
(51)	$Cl + HNO_3 \rightarrow HCl + NO_3$	$1.0 \times 10^{-11} \exp(-2170/T)$	20
(52)	$H + HCl \rightarrow H_2 + Cl$	$7.8 \times 10^{-12} \exp(-1600/T)$	20
(53)	$HCl + OH \rightarrow Cl + H_2O$	$3.0 \times 10^{-12} \exp(-425/T)$	20
(54)	$HCl + O \rightarrow Cl + OH$	$1.14 \times 10^{-11} \exp(-3370/T)$	20
(55)	$Cl + O_2 + M \rightarrow ClO_2 + M$	1.7×10^{-33}	20
(56)	$ClO_2 + M \rightarrow Cl + O_2 + M$	$5.8 \times 10^{-09} \exp(-3580/T)$	21
(57)	$2Cl + M \rightarrow Cl_2 + M$	$6.0 \times 10^{-34} \exp(900/T)$	20
(58)	$Cl + ClO_2 \rightarrow 2ClO$	1.1×10^{-11}	20
(59)	$Cl + ClO_2 \rightarrow Cl_2 + O_2$	1.6×10^{-10}	20
(60)	$2ClO + M \rightarrow Cl_2 + O_2 + M$	0	17
(61)	$Cl_2 + O \rightarrow ClO + Cl$	$4.2 \times 10^{-12} \exp(-1370/T)$	20
(62)	$Cl + ClO \rightarrow Cl_2 + O$	0	(f)
(63)	$2ClO \rightarrow ClO_2 + Cl$	$2.0 \times 10^{-12} \exp(-2200/T)$	20
(64)	$2OH + M \rightarrow H_2O_2 + M$	$1.25 \times 10^{-32} \exp(900/T)$	20
(65)	$H_2O_2 + O \rightarrow OH + HO_2$	$2.75 \times 10^{-12} \exp(-2125/T)$	20
(66)	$OH + CH_4 \rightarrow CH_3 + H_2O$	$2.36 \times 10^{-12} \exp(-1710/T)$	20
(67)	$ClO + NO_2 + M \rightarrow ClONO_2 + M$	$^g\phi_5([M],T)$	20
(68)	$HCl + ClONO_2 \rightarrow Cl_2 + HNO_3$	0	(f)
(69)	$ClONO_2 + O \rightarrow ClO + NO_3$	$3.0 \times 10^{-12} \exp(-808/T)$	20
(70)	$HO_2 + NO_2 \rightarrow HNO_2 + O_2$	2.0×10^{-15}	20
(71)	$O(^1D) + HCl \rightarrow OH + Cl$	1.4×10^{-10}	20
(72)	$H_2 + OH \rightarrow H_2O + H$	$3.6 \times 10^{-11} \exp(-2590/T)$	20
(73)	$2ClO \rightarrow Cl_2 + O2$	$5.0 \times 10^{-13} \exp(-1238/T)$	20
^{h}(74)	$O(^1D) + CF_2Cl_2 \rightarrow 2Cl + \ldots$	2.0×10^{-10}	20
^{h}(75)	$O(^1D) + CFCl_3 \rightarrow 2Cl + \ldots$	2.3×10^{-10}	20
(76)	$CH_3 + O_2 \rightarrow CH_2O + OH$	$2.9 \times 10^{-13} \exp(-940/T)$	20
(77)	$CH_3 + O_2 + M \rightarrow CH_3O_2 + M$	1.9×10^{-31}	20
(78)	$CH_3O_2 + HO_2 \rightarrow CH_3OOH + O_2$	6.7×10^{-14}	20
(79)	$CH_3O_2 + NO \rightarrow CH_3O + NO_2$	$3.3 \times 10^{-12} \exp(-500/T)$	20
(80)	$CH_3O_2 + NO \rightarrow CH_2O + HNO_2$	0	20

See footnotes at end of table, page 33.

TABLE I.- Continued

(a) Concluded

Process	Rate expression (a)	Ref.
(81) $CH_3O_2 + NO_2 \rightarrow CH_2O + HNO_3$	$0.25(k_{79}/2.2)$	22
(82) $CH_3O + O_2 \rightarrow CH_2O + HO_2$	$1.6 \times 10^{-13} \exp(-3300/T)$	20
(83) $CH_2O + OH \rightarrow HCO + H_2O$	$3.0 \times 10^{-11} \exp(-250/T)$	20
(84) $HCO + O_2 \rightarrow CO + HO_2$	5.7×10^{-12}	20
(85) $CO + OH \rightarrow CO_2 + H$	[i]$\phi_6([M])$	23
(86) $CH_3Cl + OH \rightarrow CH_2 + Cl + H_2O$	$2.2 \times 10^{-12} \exp(-1142/T)$	20
(87) $CH_3OOH + OH \rightarrow CH_3O_2 + H_2O$	k_{21}	24

[a]Bimolecular rates are in units cm^3/particle-s, termolecular rates in cm^6/particle^2-s.

[b]$\log_{10} \phi_1 = -AT/(B + T) - 0.5 \log_{10}(T/280) - \xi$ where
$$\xi = \log_{10}[M]$$
$$A = 31.62273 - 0.258304\xi - 0.0889287\xi^2 + 0.002520173\xi^3$$
$$B = -327.372 + 44.5586\xi - 1.38092\xi^2$$

[c]This expression closely approximates tabular rate function given in reference 20.

[d]$\phi_3 = (1/[M])(1.48 \times 10^{-3}) \exp(861/T)$

[e]$\phi_4 = \phi_3/(1.27 \times 10^{-27} \exp(11180/T)$

[f]Rates which are unimportant and/or for which insufficient information is available are equated to zero.

[g]$\phi_5 = (3.3 \times 10^{-23} T^{-3.34})/(1 + 8.7 \times 10^{-9} T^{-0.6}[M]^{1/2})$

[h]The only active products considered for these processes are chlorine atoms.

[i]$\phi_6 = (1.5 \times 10^{-13} + 9.316 \times 10^{-33}[M])/(1 + 1.5526 \times 10^{-20}[M])$

TABLE I.- Continued

(b) Photolytic processes

Process	Wavelength range, nm	Computed values of J, s^{-1}, at z, km, of –						Refs.
		0	8	16	25	40	55	
(1) $O_2 + h\nu \rightarrow 2O$	[a]116.3 to 235.3	0.294×10^{-23}	0.122×10^{-19}	0.587×10^{-15}	0.233×10^{-11}	0.519×10^{-9}	0.110×10^{-8}	12, 24, 25
(2) $O_3 + h\nu \rightarrow O + O_2$	116.3 to 735.0	$.380 \times 10^{-3}$	$.388 \times 10^{-3}$	$.398 \times 10^{-3}$	$.428 \times 10^{-3}$	$.461 \times 10^{-3}$	$.460 \times 10^{-3}$	12, 26
(3) $O_3 + h\nu \rightarrow O(^1D) + O_2$	116.3 to 735.0	$.154 \times 10^{-5}$	$.195 \times 10^{-5}$	$.890 \times 10^{-5}$	$.382 \times 10^{-4}$	$.183 \times 10^{-2}$	$.822 \times 10^{-2}$	12, 26
(4) $NO_2 + h\nu \rightarrow NO + O$	130.7 to 497.5	$.110 \times 10^{-1}$	$.110 \times 10^{-1}$	$.110 \times 10^{-1}$	$.112 \times 10^{-1}$	$.116 \times 10^{-1}$	$.117 \times 10^{-1}$	27
(5) $NO_2 + h\nu \rightarrow NO + O(^1D)$	130.7 to 497.5	$.641 \times 10^{-19}$	$.256 \times 10^{-15}$	$.121 \times 10^{-10}$	$.483 \times 10^{-7}$	$.157 \times 10^{-4}$	$.347 \times 10^{-4}$	28
(6) $HNO_3 + h\nu \rightarrow NO_2 + OH$	190.5 to 322.5	$.392 \times 10^{-6}$	$.412 \times 10^{-6}$	$.467 \times 10^{-6}$	$.142 \times 10^{-5}$	$.569 \times 10^{-4}$	$.990 \times 10^{-4}$	29
(7) $HNO_2 + h\nu \rightarrow NO + OH$	303.0 to 397.5	$.607 \times 10^{-3}$	$.607 \times 10^{-3}$	$.609 \times 10^{-3}$	$.618 \times 10^{-3}$	$.632 \times 10^{-3}$	$.633 \times 10^{-3}$	29
(8) $H_2O + h\nu \rightarrow H + OH$	116.3 to 198.0	$.654 \times 10^{-22}$	$.404 \times 10^{-19}$	$.466 \times 10^{-15}$	$.442 \times 10^{-11}$	$.209 \times 10^{-8}$	$.141 \times 10^{-7}$	27
(9) $H_2O_2 + h\nu \rightarrow 2OH$	175.4 to 347.5	$.783 \times 10^{-4}$	$.791 \times 10^{-4}$	$.813 \times 10^{-4}$	$.944 \times 10^{-4}$	$.213 \times 10^{-3}$	$.372 \times 10^{-3}$	30, 31
(10) $NO_3 + h\nu \rightarrow NO + O_2$	397.5 to 705.0	$.261 \times 10^{-2}$	$.262 \times 10^{-2}$	$.268 \times 10^{-2}$	$.273 \times 10^{-2}$	$.273 \times 10^{-2}$	$.273 \times 10^{-2}$	29
(11) $NO_3 + h\nu \rightarrow NO_2 + O$	397.5 to 705.0	$.261 \times 10^{-1}$	$.262 \times 10^{-1}$	$.263 \times 10^{-1}$	$.268 \times 10^{-1}$	$.273 \times 10^{-1}$	$.273 \times 10^{-1}$	29
(12) $N_2O + h\nu \rightarrow O(^1D) + N_2$	116.3 to 250.0	$.939 \times 10^{-20}$	$.111 \times 10^{-15}$	$.112 \times 10^{-11}$	$.408 \times 10^{-8}$	$.375 \times 10^{-6}$	$.632 \times 10^{-6}$	32, 33, 34
(13) $N_2O_5 + h\nu \rightarrow NO_2 + NO_3$	210.5 to 377.5	$.292 \times 10^{-4}$	$.297 \times 10^{-4}$	$.306 \times 10^{-4}$	$.371 \times 10^{-4}$	$.210 \times 10^{-3}$	$.495 \times 10^{-3}$	29
(14) $NO + h\nu \rightarrow N + O$	183.0 to 191.0	$.549 \times 10^{-48}$	$.550 \times 10^{-37}$	$.157 \times 10^{-26}$	$.460 \times 10^{-13}$	$.406 \times 10^{-6}$	$.395 \times 10^{-5}$	35
(15) $HCl + h\nu \rightarrow H + Cl$	138.9 to 219.8	$.615 \times 10^{-20}$	$.661 \times 10^{-16}$	$.276 \times 10^{-12}$	$.251 \times 10^{-8}$	$.251 \times 10^{-6}$	$.469 \times 10^{-6}$	36
(16) $ClO_2 + h\nu \rightarrow Cl + O_2$	224.7 to 281.7	$.491 \times 10^{-28}$	$.107 \times 10^{-26}$	$.128 \times 10^{-22}$	$.183 \times 10^{-13}$	$.558 \times 10^{-3}$	$.567 \times 10^{-2}$	37
(17) $ClO + h\nu \rightarrow Cl + O$	227.3 to 281.7	$.929 \times 10^{-28}$	$.139 \times 10^{-26}$	$.252 \times 10^{-24}$	$.224 \times 10^{-14}$	$.474 \times 10^{-3}$	$.381 \times 10^{-2}$	37
(18) $Cl_2 + h\nu \rightarrow 2Cl$	246.9 to 447.5	$.246 \times 10^{-2}$	$.248 \times 10^{-2}$	$.250 \times 10^{-2}$	$.262 \times 10^{-2}$	$.291 \times 10^{-2}$	$.296 \times 10^{-2}$	37, 38
(19) $CFCl_3 + h\nu \rightarrow 2.5Cl + \ldots$	185.2 to 227.3	$.136 \times 10^{-18}$	$.165 \times 10^{-14}$	$.178 \times 10^{-10}$	$.642 \times 10^{-7}$	$.605 \times 10^{-5}$	$.993 \times 10^{-5}$	39
(20) $CF_2Cl_2 + h\nu \rightarrow 2Cl + \ldots$	185.2 to 222.2	$.168 \times 10^{-19}$	$.156 \times 10^{-15}$	$.147 \times 10^{-11}$	$.564 \times 10^{-8}$	$.621 \times 10^{-6}$	$.120 \times 10^{-5}$	39
(21) $ClONO_2 + h\nu \rightarrow ClO + NO_2$	185.2 to 462.5	$.637 \times 10^{-4}$	$.644 \times 10^{-4}$	$.658 \times 10^{-4}$	$.762 \times 10^{-4}$	$.395 \times 10^{-3}$	$.931 \times 10^{-3}$	40
(22) $CCl_4 + h\nu \rightarrow 2Cl + \ldots$	185.2 to 227.3	$.173 \times 10^{-18}$	$.224 \times 10^{-14}$	$.294 \times 10^{-10}$	$.111 \times 10^{-6}$	$.158 \times 10^{-4}$	$.256 \times 10^{-4}$	41
(23) $CH_3Cl + h\nu \rightarrow CH_3 + Cl$	173.9 to 219.8	$.262 \times 10^{-20}$	$.257 \times 10^{-16}$	$.250 \times 10^{-12}$	$.944 \times 10^{-9}$	$.968 \times 10^{-7}$	$.198 \times 10^{-6}$	42
(24) $CH_2O + h\nu \rightarrow H + HCO$	289.9 to 362.5	$.320 \times 10^{-4}$	$.325 \times 10^{-4}$	$.337 \times 10^{-4}$	$.412 \times 10^{-4}$	$.730 \times 10^{-4}$	$.784 \times 10^{-4}$	43
(25) $CH_2O + h\nu \rightarrow CO + H_2$	289.9 to 362.5	$.900 \times 10^{-4}$	$.908 \times 10^{-4}$	$.922 \times 10^{-4}$	$.101 \times 10^{-3}$	$.122 \times 10^{-3}$	$.125 \times 10^{-3}$	43
(26) $HCO + h\nu \rightarrow CO + H$	(b)	0	0	0	0	0	0	----------
(27) $CH_3O_2 + h\nu \rightarrow CH_3O + O$	175.4 to 347.5	$.261 \times 10^{-4}$	$.264 \times 10^{-4}$	$.271 \times 10^{-4}$	$.315 \times 10^{-4}$	$.710 \times 10^{-4}$	$.240 \times 10^{-3}$	[c]4
(28) $CH_3OOH + h\nu \rightarrow CH_3O + OH$	175.4 to 347.5	$.783 \times 10^{-4}$	$.792 \times 10^{-4}$	$.813 \times 10^{-4}$	$.944 \times 10^{-4}$	$.213 \times 10^{-3}$	$.372 \times 10^{-3}$	[d]44

[a]Cross sections of reference 12 are used for $116.3 \leq \lambda \leq 175.4$ nm; correlations of reference 24 are used for $175.4 < \lambda \leq 204.1$ nm, and cross sections of reference 25 are used for $204.1 < \lambda \leq 235.3$ nm.

[b]This process omitted from present calculations.

[c]$J_{27} = J_9/3$ as assumed in reference 4.

[d]$J_{28} = J_9$ as assumed in reference 44.

TABLE II.- SPECIES AND BOUNDARY CONDITIONS FOR ONE-DIMENSIONAL MODEL

[P.E. denotes photochemical equilibrium]

Species	Lower boundary		Upper boundary	
	Number density, n, particles-cm^{-3}	Flux, Φ, particles-m^{-2}-s^{-1}	Number density, n, particles-m^{-3}	Flux, Φ, particles-m^{-2}-s^{-1}
O_3	6.35×10^{11}			0
$O(^3P)$	P.E.		P.E.	
NO	P.E.			0
NO_2	1.00×10^9		P.E.	
HNO_3		0		0
HNO_2		0	P.E.	
NO_3	P.E.		P.E.	
H_2O_2		0		0
OH	P.E.		P.E.	
HO_2		0	P.E.	
N_2O	8.02×10^{12}			0
N_2O_5	P.E.			0
H_2O	3.34×10^{17}			0
Cl	P.E.		P.E.	
ClO	P.E.		P.E.	
HCl	2.67×10^{10}			0
CF_2Cl_2	[a]0		[a]0	
$CFCl_3$	[a]0		[a]0	
CH_4	3.48×10^{13}			0
$ClNO_3$		0	P.E.	
CH_2O		0		0
CO	2.50×10^{12}			0
CH_3OOH		0		0
CCl_4	2.55×10^9			0
CH_3Cl	1.91×10^{10}			0

H
$O(^1D)$
N
Cl_2 } These species are computed assuming photochemical
CH_3 equilibrium at all altitudes
HCO
CH_3O_2
CH_3
ClO_2

O_2 } These species have fixed vertical profiles
H_2

[a]For the ambient atmosphere, the chlorofluoromethanes are not normally included. For injection of these species, flux boundary conditions are imposed.
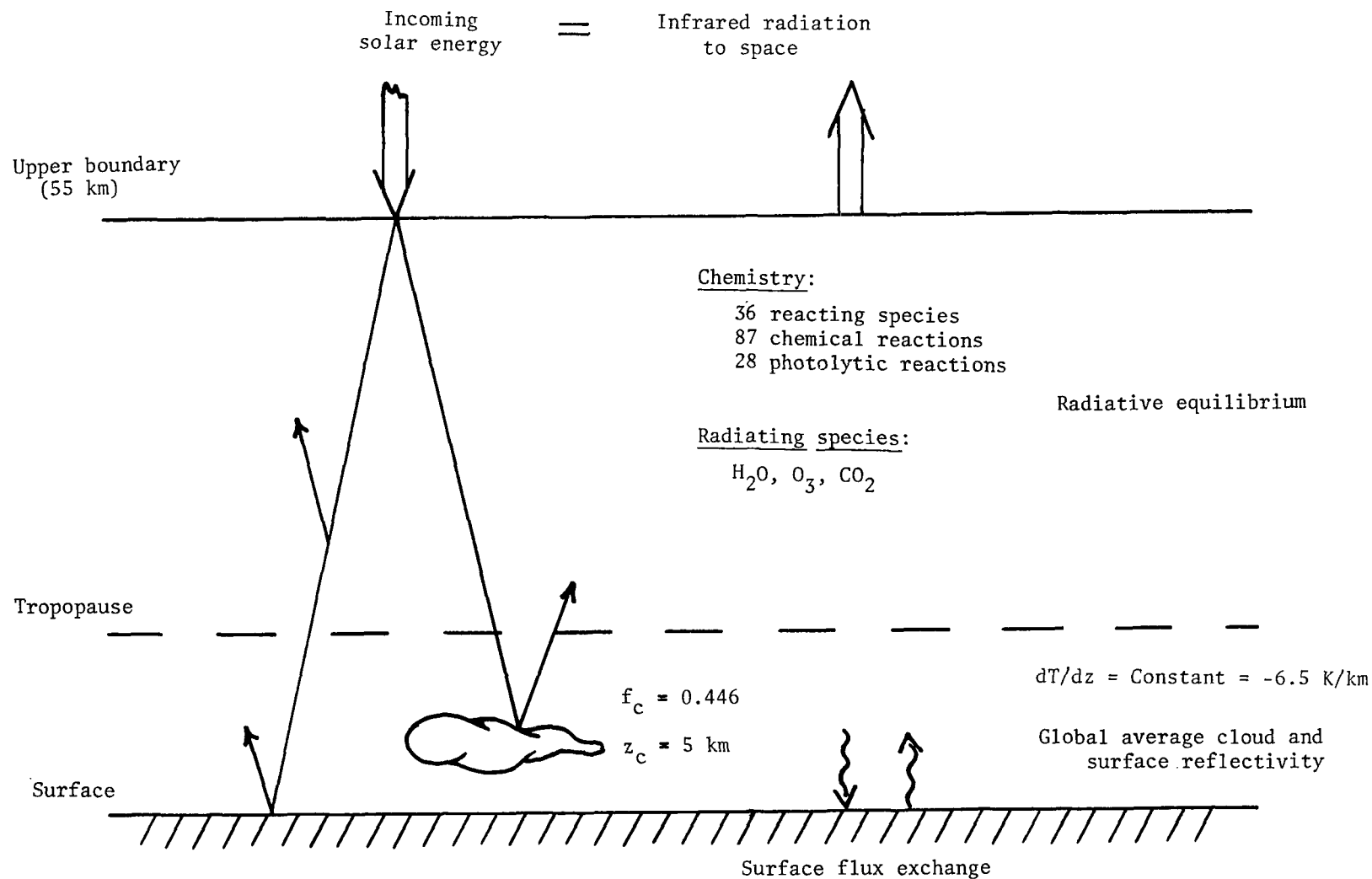
Incoming
solar energy $=$ Infrared radiation
to space

Upper boundary
(55 km)

Chemistry:

36 reacting species
87 chemical reactions
28 photolytic reactions

Radiative equilibrium

Radiating species:

H_2O, O_3, CO_2

Tropopause

$f_c = 0.446$

$dT/dz = $ Constant $= -6.5$ K/km

$z_c = 5$ km

Global average cloud and
surface reflectivity

Surface

Surface flux exchange

Figure 1.- Pictorial representation of present steady-state one-dimensional photochemical model.

Assume initial
temperature distribution

Calculate concentration
profile using temperatures
from previous step

With concentrations from
previous step calculate a
new temperature profile

Does current temperature
profile agree with previous
profile

No

Yes

Stop
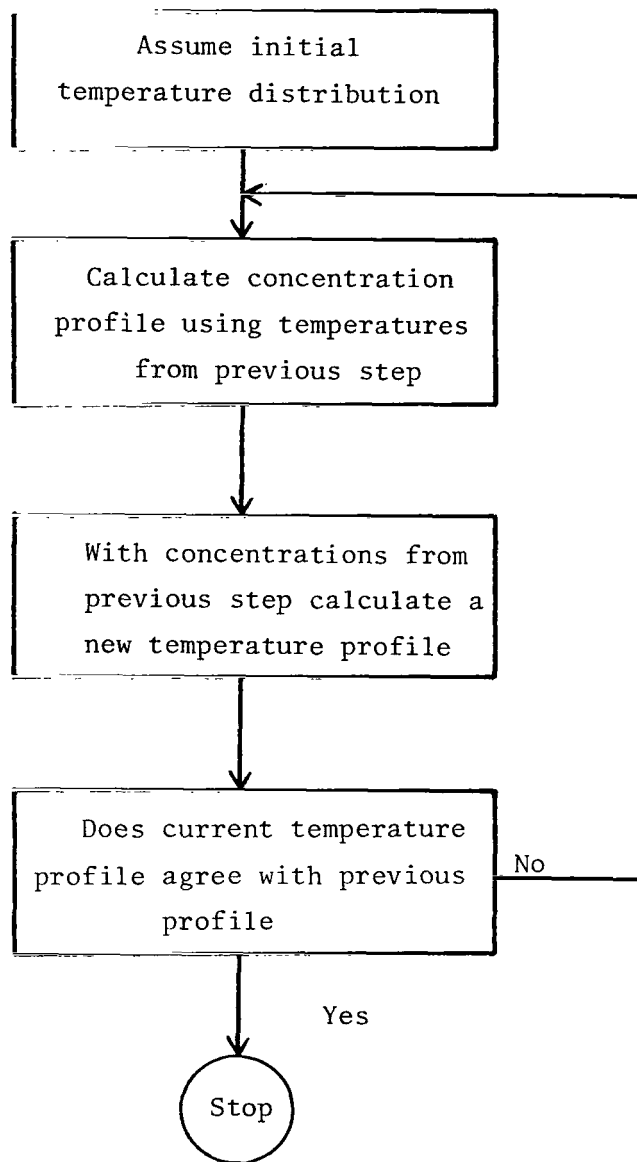
Figure 2.- Schematic illustration of computational
procedure used to include temperature-chemistry
coupling.

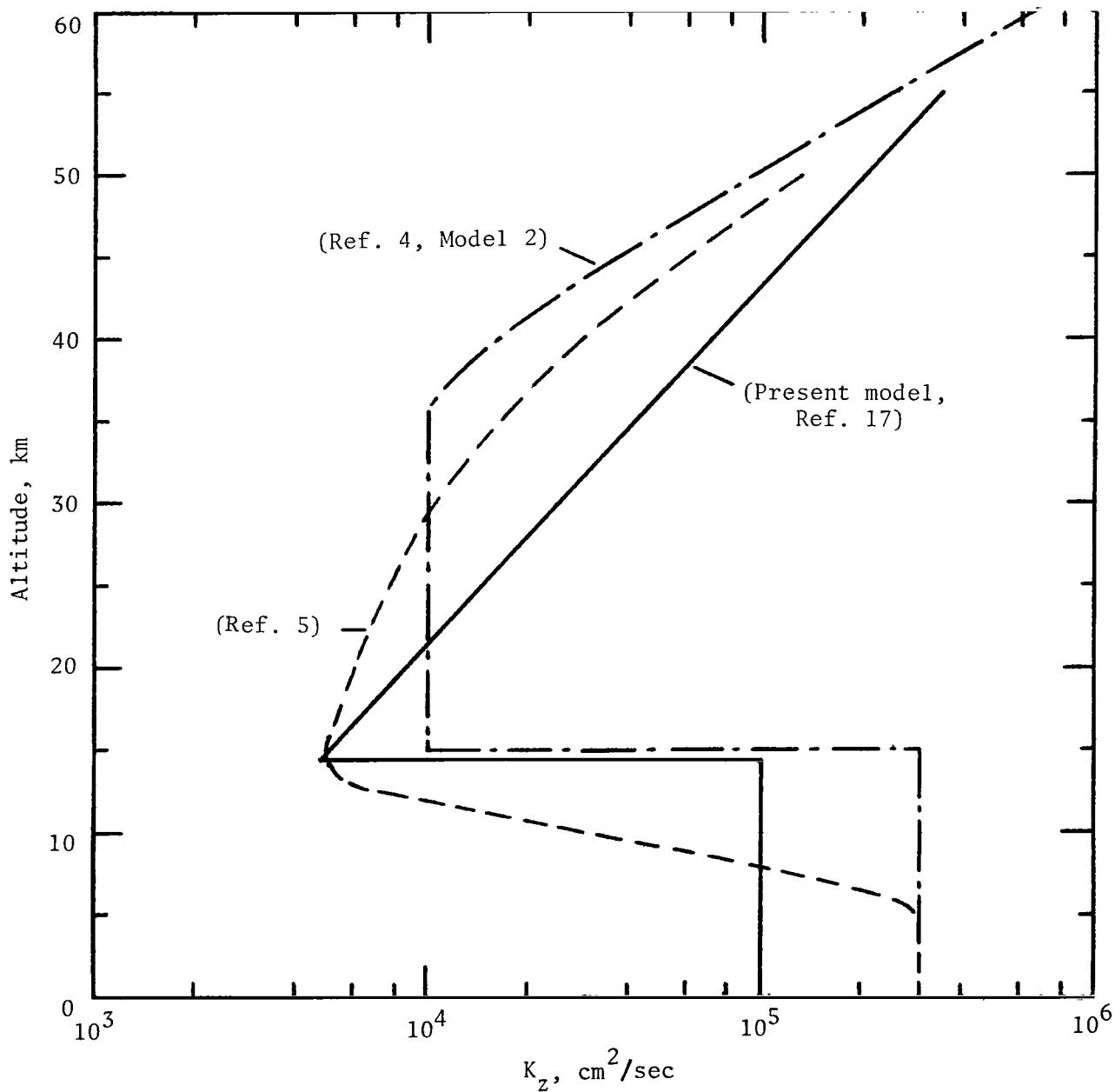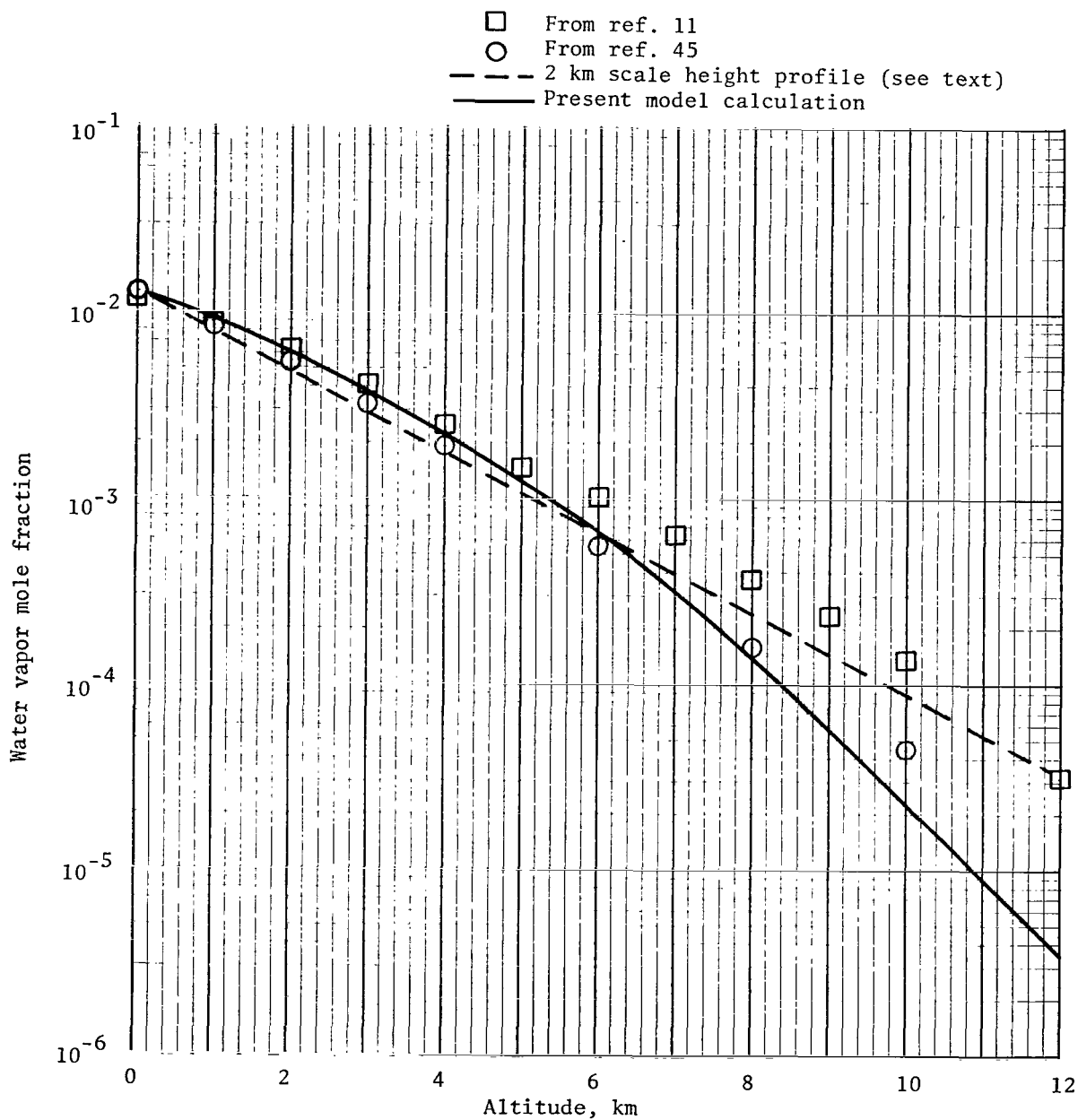Figure 3.- Typical vertical diffusion coefficients used in one-dimensional models.

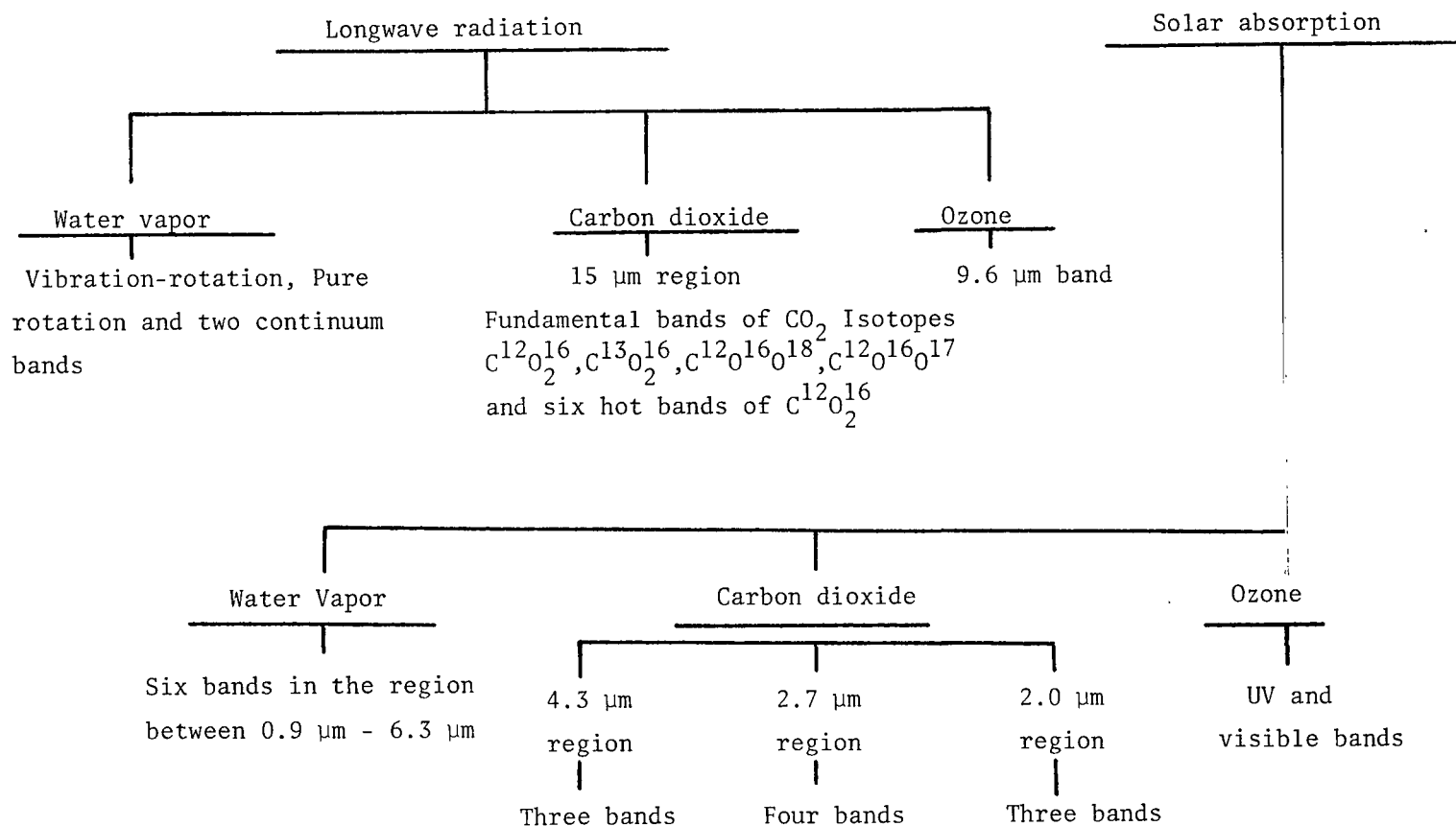Figure 4.- Vertical profiles of water vapor mole fraction.

Longwave radiation

Solar absorption

Water vapor

Vibration-rotation, Pure rotation and two continuum bands

Carbon dioxide

15 μm region

Fundamental bands of CO_2 Isotopes $C^{12}O_2^{16}, C^{13}O_2^{16}, C^{12}O^{16}O^{18}, C^{12}O^{16}O^{17}$ and six hot bands of $C^{12}O_2^{16}$

Ozone

9.6 μm band

Water Vapor

Six bands in the region between 0.9 μm - 6.3 μm

Carbon dioxide

4.3 μm region

2.7 μm region

2.0 μm region

Ozone

UV and visible bands

Three bands

Four bands

Three bands

Figure 5.- Infrared and solar absorption bands used in one-dimensional radiative transfer calculation.
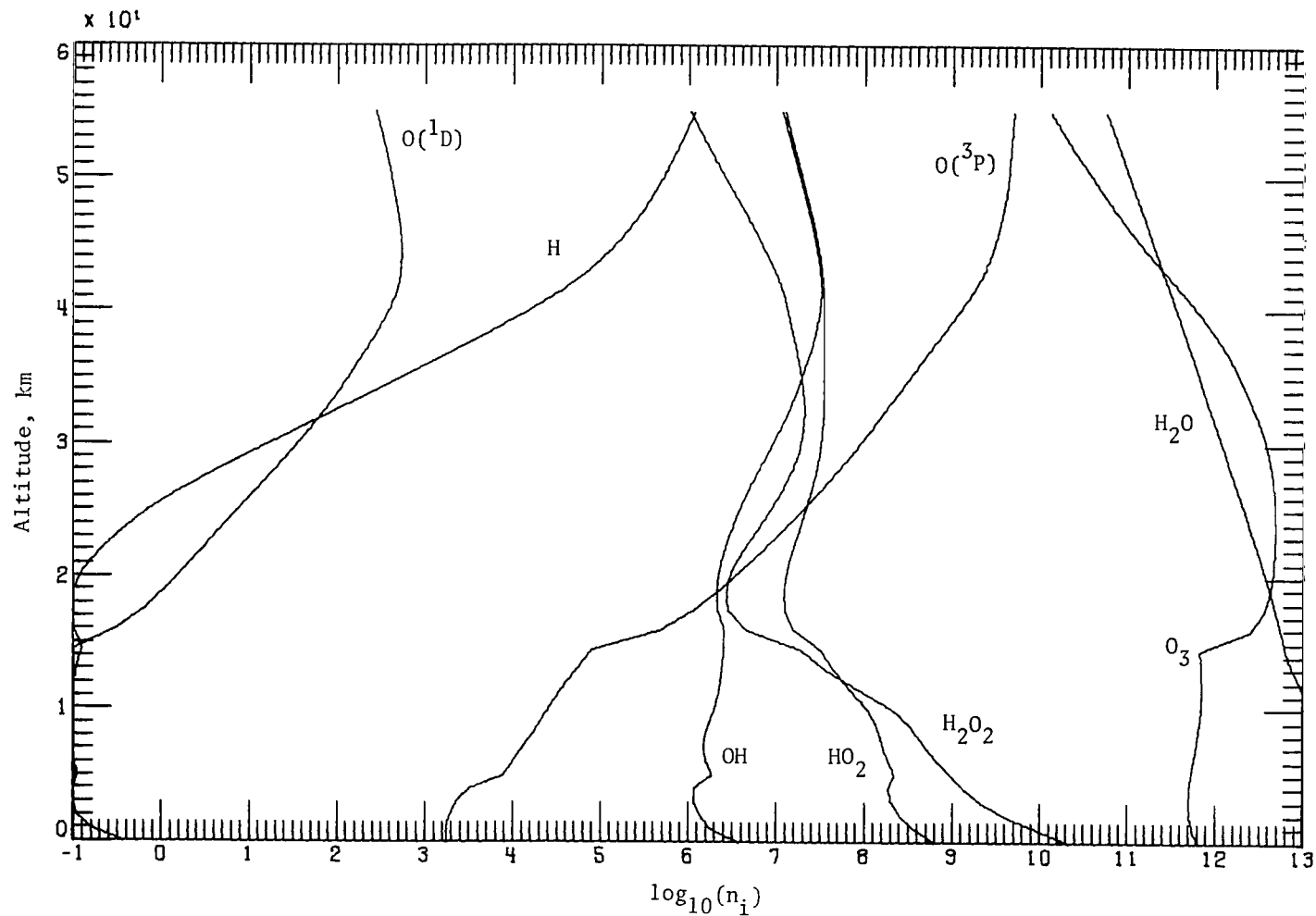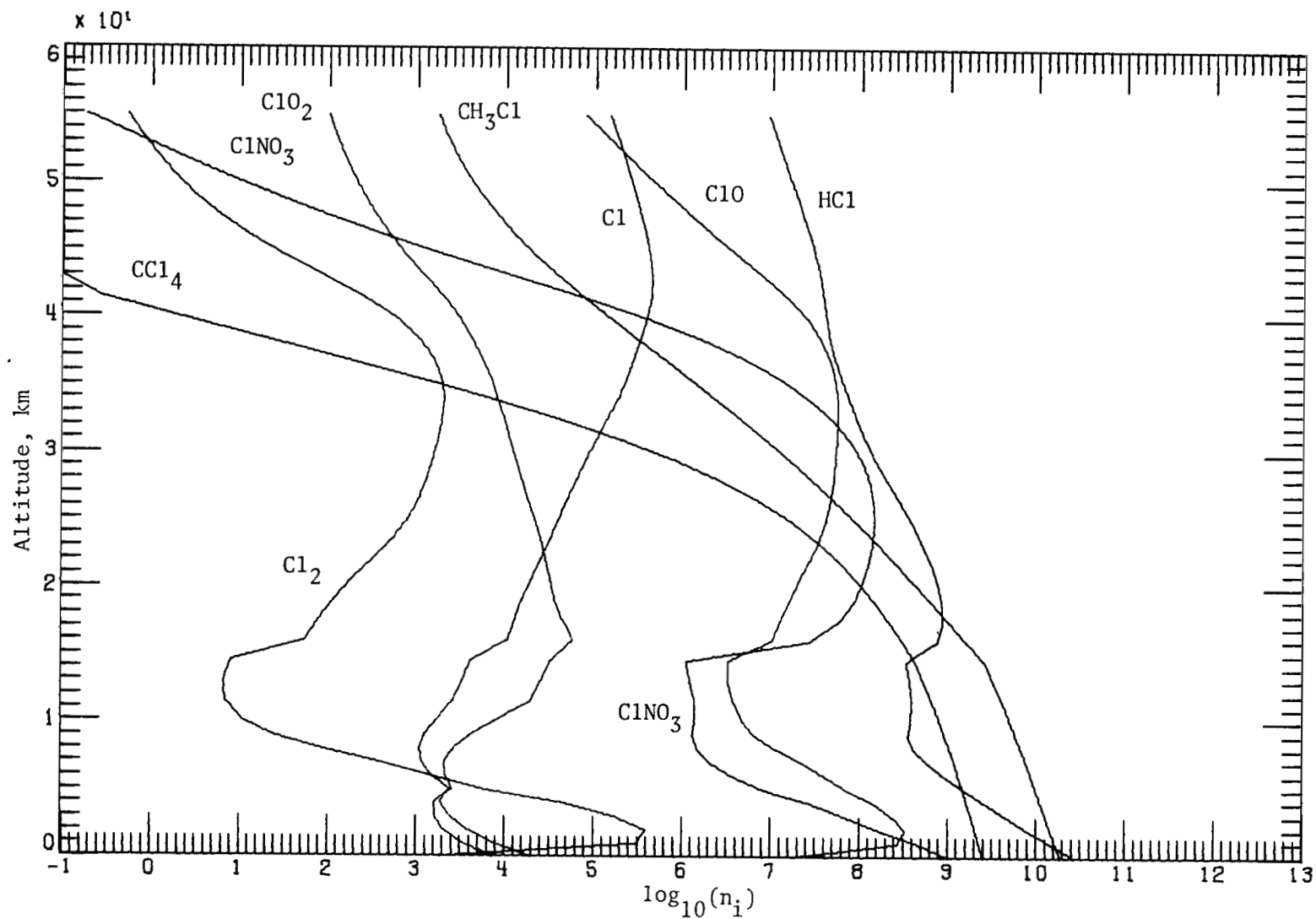
(a) Odd oxygen and HO_x species.

Figure 6.- Vertical profiles of minor atmospheric constituents as computed by the Langley photochemical model. n_i is in particles-cm^{-3}.
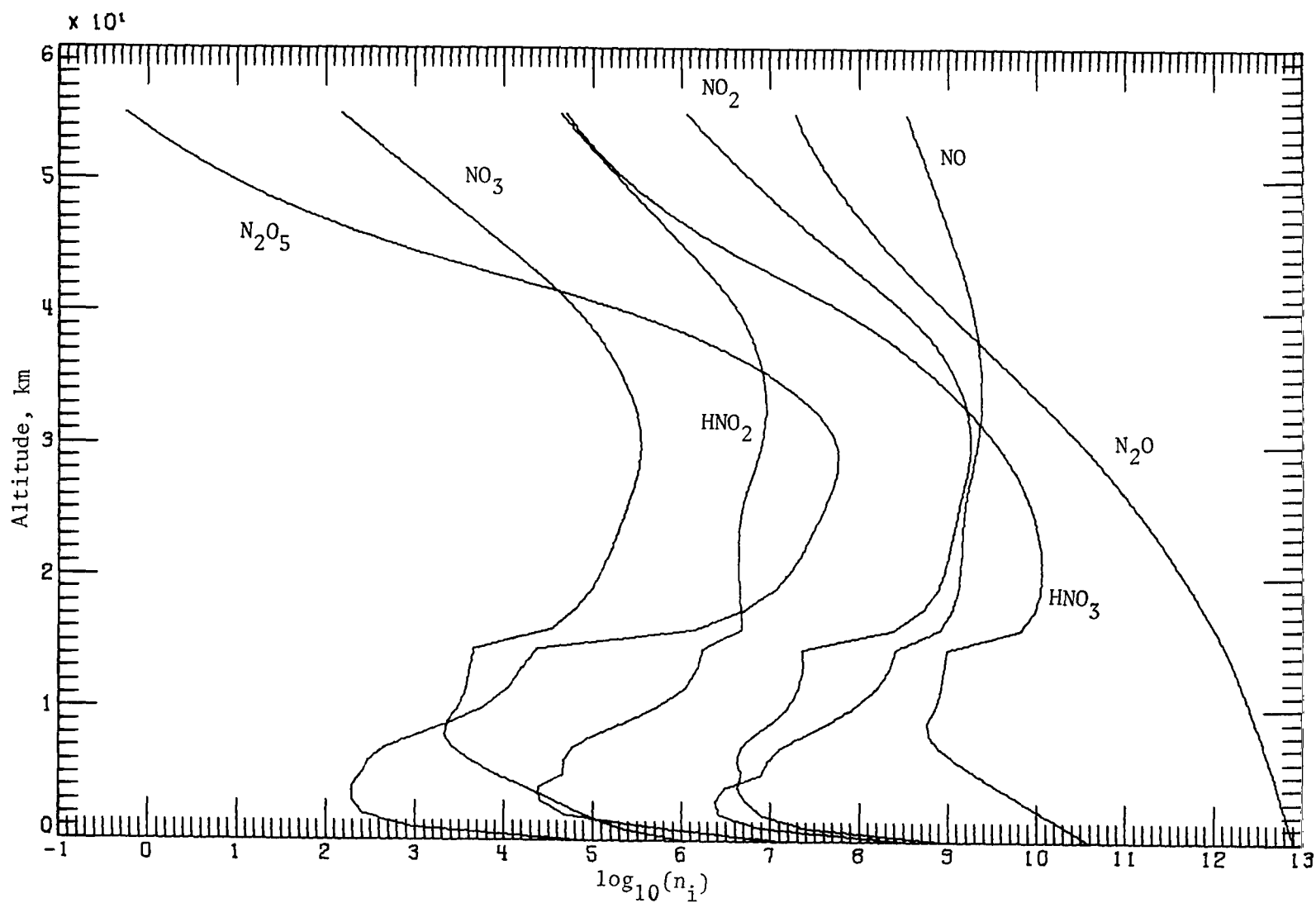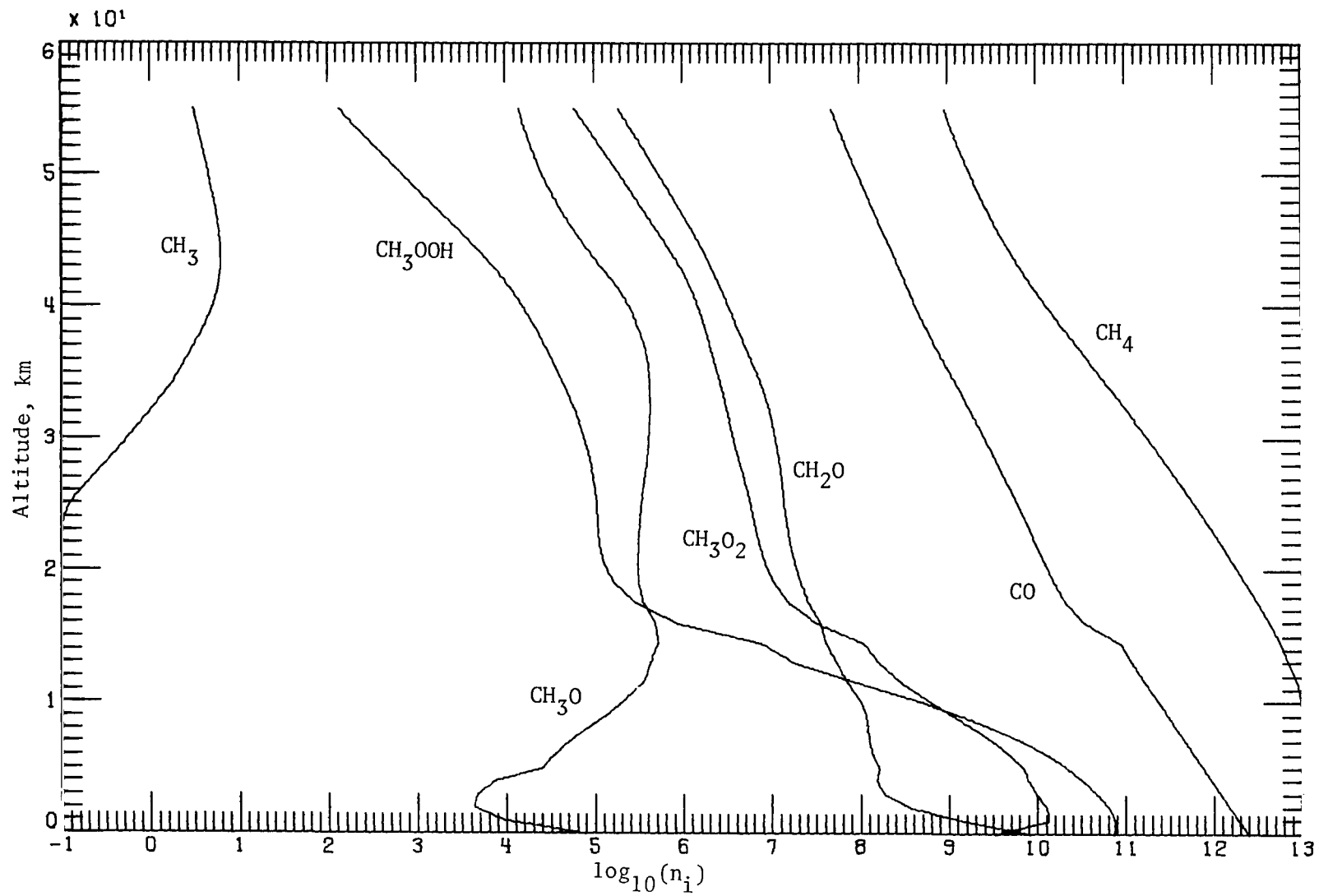
(b) Nitrogen-containing species.

Figure 6.- Continued.

(c) Chlorine-containing species.

Figure 6.- Continued.
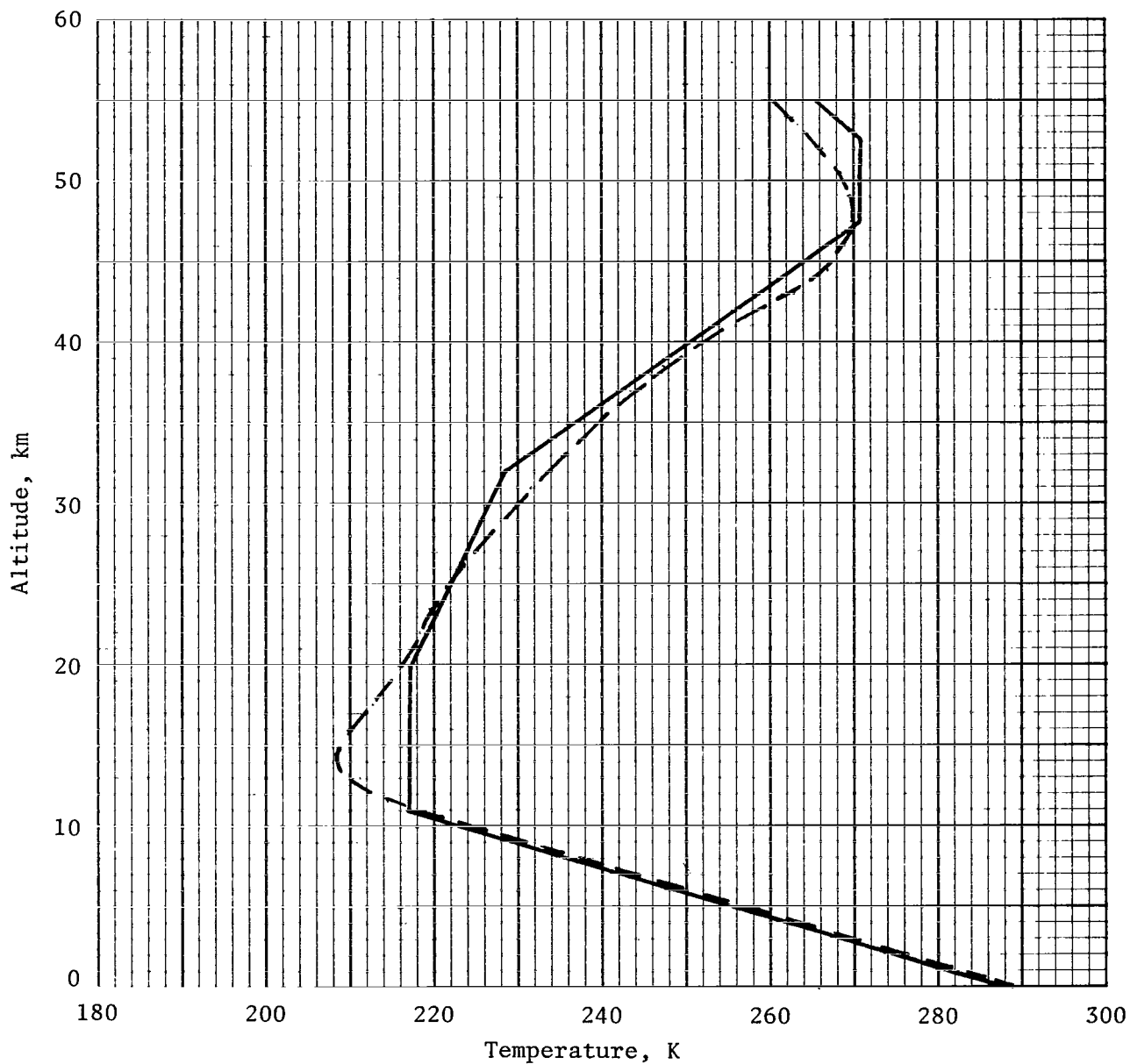
(d) Carbon-containing species.

Figure 6.- Concluded.

Figure 7.- Vertical temperature distribution (dashed curve) obtained
from coupled solution compared with U.S. Standard Atmosphere,
1962 (ref. 10) profile (solid curve).

1. Report No. NASA TP-1418	2. Government Accession No.	3. Recipient's Catalog No.
4. Title and Subtitle A COUPLED RADIATIVE-CONVECTIVE-PHOTOCHEMICAL MODEL OF THE STRATOSPHERE		5. Report Date April 1979
		6. Performing Organization Code
7. Author(s) Robert E. Boughner and John E. Nealy		8. Performing Organization Report No. L-12659
9. Performing Organization Name and Address NASA Langley Research Center Hampton, VA 23665		10. Work Unit No. 198-30-02-01
		11. Contract or Grant No.
12. Sponsoring Agency Name and Address National Aeronautics and Space Administration Washington, DC 20546		13. Type of Report and Period Covered Technical Paper
		14. Sponsoring Agency Code

15. Supplementary Notes

16. Abstract

A one-dimensional atmospheric model is described. The neutral photochemical processes of the troposphere and stratosphere are presented by a reaction set of 87 kinetic processes and 28 photolytic reactions, with vertical transport being taken into account by an eddy diffusion parameter. The vertical temperature profiles are coupled with the chemical calculations by means of a radiative-convective code. The model has the capability of including effects of multiple scattering and diurnal variations in species concentrations. The numerical solution methodology is described in detail, and current input data are given along with results obtained in a sample calculation.

17. Key Words (Suggested by Author(s)) Geophysics Atmospheric chemistry	18. Distribution Statement Unclassified - Unlimited Subject Category 42

19. Security Classif. (of this report) Unclassified	20. Security Classif. (of this page) Unclassified	21. No. of Pages 45	22. Price* $4.50

National Aeronautics and
Space Administration

Washington, D.C.
20546

Official Business
Penalty for Private Use, $300

THIRD-CLASS BULK RATE

U.S.MAIL

2   1 1U,E,   040979 S00903DS
DEPT OF THE AIR FORCE
AF WEAPONS LABORATORY
ATTN: TECHNICAL LIBRARY (SUL)
KIRTLAND AFB NM 87117

NASA

S

POSTMASTER: If Undeliverable (Section 158
                Postal Manual) Do Not Return